

AMADEUS – The Acoustic Neutrino Detection Test System of the ANTARES Deep-Sea Neutrino Telescope

J.A. Aguilar^a, I. Al Samarai^b, A. Albert^c, M. Anghinolfi^d,
 G. Anton^e, S. Anvar^f, M. Ardid^g, A.C. Assis Jesus^h,
 T. Astraatmadja^{h,1}, J-J. Aubert^b, R. Auer^e, E. Barbaritoⁱ, B. Baret^j,
 S. Basa^k, M. Bazzotti^{ℓ,m}, V. Bertin^b, S. Biagi^{ℓ,m}, C. Bigongiari^a,
 M. Bou-Cabo^g, M.C. Bouwhuis^h, A. Brown^b, J. Brunner^{b,2},
 J. Busto^b, F. Camarena^g, A. Capone^{n,o}, C. Cârloganu^p,
 G. Carminati^{ℓ,m}, J. Carr^b, B. Cassanoⁱ, E. Castorina^{q,r},
 V. Cavasinni^{q,r}, S. Cecchini^{m,s}, A. Ceresⁱ, Ph. Charvis^t,
 T. Chiarusi^m, N. Chon Sen^c, M. Circellaⁱ, R. Coniglione^u,
 H. Costantini^d, N. Cottini^v, P. Coyle^b, C. Curtil^b, G. De Bonis^{n,o},
 M.P. Decowski^h, I. Dekeyser^w, A. Deschamps^t, C. Distefano^u,
 C. Donzaud^{j,x}, D. Dornic^{b,a}, D. Drouhin^c, T. Eberl^e,
 U. Emanuele^a, J-P. Ernenwein^b, S. Escoffier^b, F. Fehr^e,
 C. Fiorelloⁱ, V. Flaminio^{q,r}, U. Fritsch^e, J-L. Fuda^w, P. Gay^p,
 G. Giacomelli^{ℓ,m}, J.P. Gómez-González^a, K. Graf^e, G. Guillard^y,
 G. Halladjian^b, G. Hallewell^b, H. van Haren^z, A.J. Heijboer^h,
 E. Heine^h, Y. Hello^t, J.J. Hernández-Rey^a, B. Herold^e, J. Höbl^e,
 M. de Jong^{h,1}, N. Kalantar-Nayestanaki^{aa}, O. Kalekin^e,
 A. Kappes^e, U. Katz^e, P. Keller^b, P. Kooijman^{h,ab,ac}, C. Kopper^e,
 A. Kouchner^j, W. Kretschmer^e, R. Lahmann^{e,*}, P. Lamare^f,
 G. Lambard^b, G. Larosa^g, H. Laschinsky^e, H. Le Provost^f,
 D. Lefèvre^w, G. Lelaizant^b, G. Lim^{h,ac}, D. Lo Presti^{ad},
 H. Loehner^{aa}, S. Loucatos^v, F. Louis^f, F. Lucarelli^{n,o},
 S. Mangano^a, M. Marcellin^k, A. Margiotta^{ℓ,m},
 J.A. Martinez-Mora^g, A. Mazure^k, M. Mongelliⁱ, T. Montaruli^{i,ae},
 M. Morganti^{q,r}, L. Moscoso^{v,j}, H. Motz^e, C. Naumann^{v,4},
 M. Neff^e, R. Ostasch^e, D. Palioselitis^h, G.E.Păvălaș^{af}, P. Payre^b,
 J. Petrovic^h, N. Picot-Clemente^b, C. Picq^v, V. Popa^{af}, T. Pradier^y,
 E. Presani^h, C. Racca^c, A. Radu^{af}, C. Reed^{b,h}, G. Riccobene^u,

C. Richardt^e, M. Rujoiu^{af}, M. Ruppi^{i,3}, G.V. Russo^{ad}, F. Salesa^a,
P. Sapienza^u, F. Schöck^e, J-P. Schuller^v, R. Shanidze^e,
F. Simeone^o, M. Spurio^{ℓ,m}, J.J.M. Steijger^h, Th. Stolarczyk^v,
M. Taiuti^{ag,d}, C. Tamburini^w, L. Tasca^k, S. Toscano^a, B. Vallage^v,
V. Van Elewyck^j, G. Vannoni^v, M. Vecchi^{n,b}, P. Vernin^v,
G. Wijnker^h, E. de Wolf^{h,ac}, H. Yepes^a, D. Zaborov^{ah},
J.D. Zornoza^a, J. Zúñiga^a

- ^a*IFIC - Instituto de Física Corpuscular, Edificios Investigación de Paterna, CSIC - Universitat de València, Apdo. de Correos 22085, 46071 Valencia, Spain*
- ^b*CPPM - Centre de Physique des Particules de Marseille, CNRS/IN2P3 et Université de la Méditerranée, 163 Avenue de Luminy, Case 902, 13288 Marseille Cedex 9, France*
- ^c*GRPHE - Institut universitaire de technologie de Colmar, 34 rue du Grillenbreit BP 50568, 68008 Colmar, France*
- ^d*INFN - Sezione di Genova, Via Dodecaneso 33, 16146 Genova, Italy*
- ^e*Friedrich-Alexander-Universität Erlangen-Nürnberg, Erlangen Centre for Astroparticle Physics, Erwin-Rommel-Str. 1, 91058 Erlangen, Germany*
- ^f*Direction des Sciences de la Matière - Institut de recherche sur les lois fondamentales de l'Univers - Service d'Electronique des Détecteurs et d'Informatique, CEA Saclay, 91191 Gif-sur-Yvette Cedex, France*
- ^g*Institut d'Investigació per a la Gestió Integrada de Zones Costaneres (IGIC) - Universitat Politècnica de València. C/ Paraninf 1. , 46730 Gandia, Spain.*
- ^h*FOM Instituut voor Subatomaire Fysica Nikhef, Science Park 105, 1098 XG Amsterdam, The Netherlands*
- ⁱ*INFN - Sezione di Bari, Via E. Orabona 4, 70126 Bari, Italy*
- ^j*APC - Laboratoire AstroParticule et Cosmologie, UMR 7164 (CNRS, Université Paris 7 Diderot, CEA, Observatoire de Paris) 10, rue Alice Domon et Léonie Duquet, 75205 Paris Cedex 13, France*
- ^k*LAM - Laboratoire d'Astrophysique de Marseille, Pôle de l'Étoile Site de Château-Gombert, rue Frédéric Joliot-Curie 38, 13388 Marseille Cedex 13, France*
- ^l*Dipartimento di Fisica dell'Università, Viale Berti Pichat 6/2, 40127 Bologna, Italy*
- ^m*INFN - Sezione di Bologna, Viale Berti Pichat 6/2, 40127 Bologna, Italy*
- ⁿ*Dipartimento di Fisica dell'Università La Sapienza, P.le Aldo Moro 2, 00185 Roma, Italy*
- ^o*INFN - Sezione di Roma, P.le Aldo Moro 2, 00185 Roma, Italy*
- ^p*Clermont Université, Université Blaise Pascal, CNRS/IN2P3, Laboratoire de Physique Corpusculaire, BP 10448, 63000 Clermont-Ferrand, France*
- ^q*Dipartimento di Fisica dell'Università, Largo B. Pontecorvo 3, 56127 Pisa, Italy*
- ^r*INFN - Sezione di Pisa, Largo B. Pontecorvo 3, 56127 Pisa, Italy*
- ^s*INAF-IASF, via P. Gobetti 101, 40129 Bologna, Italy*
- ^t*Géoazur - Université de Nice Sophia-Antipolis, CNRS/INSU, IRD, Observatoire de la Côte d'Azur and Université Pierre et Marie Curie, BP 48, 06235 Villefranche-sur-mer, France*
- ^u*INFN - Laboratori Nazionali del Sud (LNS), Via S. Sofia 62, 95123 Catania, Italy*
- ^v*Direction des Sciences de la Matière - Institut de recherche sur les lois fondamentales de l'Univers - Service de Physique des Particules, CEA Saclay, 91191 Gif-sur-Yvette Cedex, France*
- ^w*COM - Centre d'Océanologie de Marseille, CNRS/INSU et Université de la Méditerranée, 163 Avenue de Luminy, Case 901, 13288 Marseille Cedex 9, France*
- ^x*Université Paris-Sud 11 - Département de Physique, 91403 Orsay Cedex, France*
- ^y*IPHC - Institut Pluridisciplinaire Hubert Curien - Université de Strasbourg et CNRS/IN2P3 23 rue du Loess, BP 28, 67037 Strasbourg Cedex 2, France*
- ^z*Royal Netherlands Institute for Sea Research (NIOZ), Landsdiep 4,1797 SZ 't Horntje (Texel), The Netherlands*
- ^{aa}*Kernfysisch Versneller Instituut (KVI), University of Groningen, Zernikelaan 25, 9747 AA Groningen, The Netherlands*
- ^{ab}*Universiteit Utrecht, Faculteit Betawetenschappen, Princetonplein 5, 3584 CC Utrecht, The Netherlands*
- ^{ac}*Universiteit van Amsterdam, Instituut voor Hoge-Energie Fysika, Science Park 105, 1098 XG Amsterdam, The Netherlands*
- ^{ad}*Dipartimento di Fisica ed Astronomia dell'Università, Viale Andrea Doria 6, 95125 Catania, Italy*
- ^{ae}*University of Wisconsin - Madison, 53715, WI, USA*
- ^{af}*Institute for Space Sciences, R-77125 Bucharest, Măgurele, Romania*
- ^{ag}*Dipartimento di Fisica dell'Università, Via Dodecaneso 33, 16146 Genova, Italy*

Abstract

The AMADEUS (ANTARES Modules for the Acoustic Detection Under the Sea) system which is described in this article aims at the investigation of techniques for acoustic detection of neutrinos in the deep sea. It is integrated into the ANTARES neutrino telescope in the Mediterranean Sea. Its acoustic sensors, installed at water depths between 2050 and 2300 m, employ piezo-electric elements for the broad-band recording of signals with frequencies ranging up to 125 kHz. The typical sensitivity of the sensors is around -145 dB re $1\text{V}/\mu\text{Pa}$ (including preamplifier). Completed in May 2008, AMADEUS consists of six “acoustic clusters”, each comprising six acoustic sensors that are arranged at distances of roughly 1 m from each other. Two vertical mechanical structures (so-called lines) of the ANTARES detector host three acoustic clusters each. Spacings between the clusters range from 14.5 to 340 m. Each cluster contains custom-designed electronics boards to amplify and digitise the acoustic signals from the sensors. An on-shore computer cluster is used to process and filter the data stream and store the selected events. The daily volume of recorded data is about 10 GB. The system is operating continuously and automatically, requiring only little human intervention. AMADEUS allows for extensive studies of both transient signals and ambient noise in the deep sea, as well as signal correlations on several length scales and localisation of acoustic point sources. Thus the system is excellently suited to assess the background conditions for the measurement of the bipolar pulses expected to originate from neutrino interactions.

Key words: AMADEUS, ANTARES, Neutrino telescope, Acoustic neutrino detection, Thermo-acoustic model

PACS: 95.55.Vj, 95.85.Ry, 13.15.+g, 43.30.+m

1 Introduction

2 Measuring acoustic pressure pulses in huge underwater acoustic arrays is a promis-
3 ing approach for the detection of cosmic neutrinos with energies exceeding 100 PeV.
4 The pressure signals are produced by the particle cascades that evolve when neu-
5 trinos interact with nuclei in water. The resulting energy deposition in a cylindri-
6 cal volume of a few centimetres in radius and several metres in length leads to

* Corresponding author; Tel.: +49 9131 8527147

Email address: robert.lahmann@physik.uni-erlangen.de (R. Lahmann).

¹ Also at University of Leiden, the Netherlands

² On leave at DESY, Platanenallee 6, 15738 Zeuthen, Germany

³ Now at Altran Italia, Corso Sempione 66, 20100 Milano, Italy

⁴ Now at LPNHE - Laboratoire de Physique Nucléaire et des Hautes Énergies, UMR 7585, 4 place Jussieu - 75252 Paris Cedex 05, France

7 a local heating of the medium which is instantaneous with respect to the hydro-
8 dynamic time scales. This temperature change induces an expansion or contrac-
9 tion of the medium depending on its volume expansion coefficient. According to
10 the thermo-acoustic model [1,2], the accelerated motion of the heated volume—a
11 micro-explosion—forms a pressure pulse of bipolar shape which propagates in the
12 surrounding medium. Coherent superposition of the elementary sound waves, pro-
13 duced over the volume of the energy deposition, leads to a propagation within a
14 flat disk-like volume (often referred to as *pancake*) in the direction perpendicular
15 to the axis of the particle cascade. After propagating several hundreds of metres
16 in sea water, the pulse has a characteristic frequency spectrum that is expected to
17 peak around 10 kHz [3–5]. Given the strongly anisotropic propagation pattern of the
18 sound waves, the details of the pressure pulse, namely its amplitude, asymmetry and
19 frequency spectrum, depend on the distance and angular position of the observer
20 with respect to the particle cascade induced by the neutrino interaction [3]. Besides
21 sea water, which is the medium under investigation in the case of the AMADEUS
22 (ANTARES Modules for the Acoustic Detection Under the Sea) project, ice [6]
23 and fresh water [7] are investigated as media for acoustic detection of neutrinos.
24 Studies in sea water are also pursued by other groups using military arrays of hy-
25 drophones (i.e. underwater microphones) [8,9] or exploiting other existing deep sea
26 infrastructures [10].

27 Two major advantages over an optical neutrino telescope motivate studying acous-
28 tic detection. First, the attenuation length in sea water is about 5 km (1 km) for
29 10 kHz (20 kHz) signals. This is one to two orders of magnitude larger than for
30 visible light with a maximum attenuation length of about 60 m. The second advan-
31 tage is the more compact sensor design and simpler readout electronics for acoustic
32 measurements. Since on the other hand the speed of sound⁵ is small compared to
33 the speed of light, coincidence windows between two spatially separated sensors
34 are correspondingly large. Furthermore, the signal amplitude is relatively small
35 compared to the acoustic background in the sea, resulting in a high trigger rate
36 at the level of individual sensors and making the implementation of efficient online
37 data reduction techniques essential. To reduce the required processing time with-
38 out sacrificing the advantages given by the large attenuation length, the concept
39 of spatially separated clusters of acoustic sensors is used in AMADEUS. Online
40 data filtering is then predominantly applied to the closely arranged sensors within
41 a cluster.

42 The AMADEUS project was conceived to perform a feasibility study for a potential
43 future large-scale acoustic neutrino detector. For this purpose, a dedicated array of
44 acoustic sensors was integrated into the ANTARES neutrino telescope [11,12]. In
45 the context of AMADEUS, the following aims are being pursued:

⁵ The speed of sound in sea water depends on temperature, salinity and pressure, i.e. depth. A good guideline value for the speed of sound at the location of AMADEUS is 1500 m/s.

- 46 • Long-term background investigations (levels of ambient noise, spatial and tem-
47 poral distributions of sources, rate of neutrino-like signals);
- 48 • Investigation of spatial correlations for transient signals and for persistent back-
49 ground on different length scales;
- 50 • Development and tests of data filter and reconstruction algorithms;
- 51 • Investigation of different types of acoustic sensors and sensing methods;
- 52 • Studies of hybrid (acoustic and optical) detection methods.

53 In particular the knowledge of the rate and correlation length of neutrino-like acous-
54 tic background events is a prerequisite for estimating the sensitivity of a future
55 acoustic neutrino detector.

56 The focus of this paper is the AMADEUS system within the ANTARES detector.
57 In Section 2, an overview of the system is given, with particular emphasis on its
58 integration into the ANTARES detector. In Section 3, the system components are
59 described and in Section 4 the system performance is discussed. The characteristic
60 features of the AMADEUS system are mainly determined by the acoustic sensors
61 and the custom-designed electronics board, which performs the off-shore process-
62 ing of the analogue signals from the acoustic sensors. These two components are
63 discussed in detail in Subsections 3.1 and 3.4.

64 **2 Overview of the AMADEUS System**

65 *2.1 The ANTARES Detector and its Sub-system AMADEUS*

66 AMADEUS is integrated into the ANTARES neutrino telescope [11,12], which was
67 designed to detect neutrinos by measuring the Cherenkov light emitted along the
68 tracks of relativistic secondary muons generated in neutrino interactions. A sketch
69 of the detector, with the AMADEUS modules highlighted, is shown in Figure 1.
70 The detector is located in the Mediterranean Sea at a water depth of about 2500 m,
71 about 40 km south of the town of Toulon on the French coast and was completed in
72 May 2008. It comprises 12 vertical structures, the *detection lines*. Each detection
73 line holds up to 25 *storeys* that are arranged at equal distances of 14.5 m along the
74 line, starting at about 100 m above the sea bed and interlinked by electro-optical
75 cables. A standard storey consists of a titanium support structure, holding three
76 *Optical Modules* [13] (each one consisting of a photomultiplier tube (PMT) inside
77 a water-tight pressure-resistant glass sphere) and one *Local Control Module (LCM)*.
78 The LCM consists of a cylindrical titanium container and the off-shore electronics
79 within that container (see Subsection 3.3).

80 A 13th line, called *Instrumentation Line (IL)*, is equipped with instruments for mon-
81 itoring the environment. It holds six storeys. For two pairs of consecutive storeys

82 in the IL, the vertical distance is increased to 80 m. Each line is fixed on the sea
 83 floor by an anchor equipped with electronics and held taut by an immersed buoy.
 84 An interlink cable connects each line to the *Junction Box* from where the main
 85 electro-optical cable provides the connection to the shore station.

86 The ANTARES lines are free to swing and twist in the undersea current. In order
 87 to determine the positions of the storey with a precision of about 20 cm—which is
 88 necessary to achieve the required pointing precision for neutrino astronomy—the
 89 detector is equipped with an acoustic positioning system [14]. The system employs
 90 an acoustic transceiver at the anchor of each line and four autonomous transpon-
 91 ders positioned around the 13 lines. Along each detection line, five positioning
 92 hydrophones receive the signals emitted by the transceivers. By performing mul-
 93 tiple time delay measurements and using these to triangulate the positions of the
 94 individual hydrophones, the line shapes can be reconstructed relative to the posi-
 95 tions of the emitters. Currently, the sequence of positioning emissions is repeated
 96 every 2 minutes.

97 In AMADEUS, acoustic sensing is integrated in the form of *acoustic storeys* that
 98 are modified versions of standard ANTARES storeys, in which the Optical Modules
 99 are replaced by custom-designed acoustic sensors. Dedicated electronics is used for
 100 the digitisation and pre-processing of the analogue signals. The acoustic storeys are
 101 equivalent to the acoustic clusters introduced in Section 1.

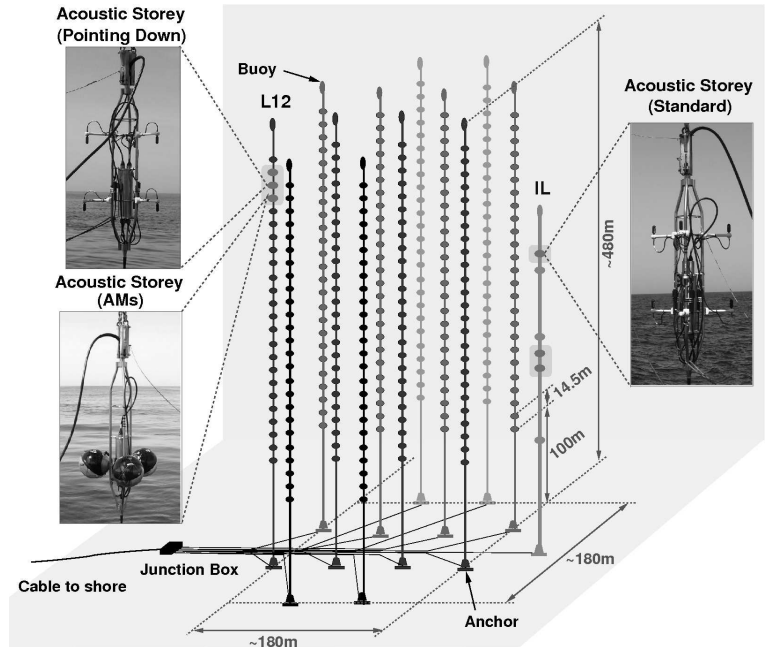


Figure 1. A sketch of the ANTARES detector. The six acoustic storeys are highlighted and their three different setups are shown (see text for details). L12 and IL denote the 12th detection line and the Instrumentation Line, respectively.

102 The AMADEUS system comprises a total of six acoustic storeys: three on the IL,
 103 which started data taking in December 2007, and three on the 12th detection line

104 (Line 12), which was connected to shore in May 2008. AMADEUS is now fully
105 functional and routinely taking data with 34 sensors. Two out of 36 hydrophones
106 became inoperational during their deployment. In both cases, the defect was due to
107 pressurisation.

108 The acoustic storeys on the IL are located at 180 m, 195 m, and 305 m above the sea
109 floor. On Line 12, which is anchored at a horizontal distance of about 240 m from
110 the IL, the acoustic storeys are positioned at heights of 380 m, 395 m, and 410 m
111 above the sea floor. With this setup, the maximum distance between two acoustic
112 storeys is 340 m. AMADEUS hence covers three length scales: spacings of the or-
113 der of 1 m between sensors within a storey (i.e. an acoustic cluster); intermediate
114 distances of 14.5 m between adjacent acoustic storeys within a line; and large scales
115 from about 100 m vertical distance on the IL up to 340 m between storeys on dif-
116 ferent lines. The sensors within a cluster allow for efficient triggering of transient
117 signals and for direction reconstruction. The combination of the direction infor-
118 mation from different acoustic storeys yields (after verifying the consistency of the
119 signal arrival times at the respective storeys) the position of an acoustic source [15].
120 The AMADEUS system includes time synchronisation and a continuously operat-
121 ing data acquisition setup and is in principle scalable to a large-volume detector.

122 2.2 *Acoustic Storeys*

123 Two types of sensing devices are used in AMADEUS: hydrophones and *Acoustic*
124 *Modules* (AMs). The sensing principle is in both cases based on the piezo-electric
125 effect and is discussed in Subsection 3.1. For the hydrophones, the piezo elements
126 are coated in polyurethane, whereas for the AMs they are glued to the inside of stan-
127 dard glass spheres which are normally used for Optical Modules. Figure 2 shows
128 the design of a standard acoustic storey with hydrophones.

129 Figure 3 shows the three different designs of acoustic storeys installed in AMADEUS.
130 The acoustic storeys on the IL house hydrophones only, whereas the lowermost
131 acoustic storey of Line 12 holds AMs. The hydrophones are mounted to point up-
132 wards, except for the central acoustic storey of Line 12, where they point down-
133 wards. The sensitivity of the hydrophones is largely reduced at their cable junctions
134 and therefore shows a strong dependence on the polar angle. The different config-
135 urations allow for investigating the anisotropy of ambient noise, which is expected
136 to originate mainly from the sea surface.

137 Three of the five storeys holding hydrophones are equipped with commercial mod-
138 els, dubbed “HTI hydrophones”⁶, and the other two with hydrophones, described
139 in detail in Subsection 3.1, developed and produced at the Erlangen Centre for As-
140 troparticle Physics (ECAP).

⁶ Custom produced by High Tech Inc (HTI) in Gulfport, MS (USA).

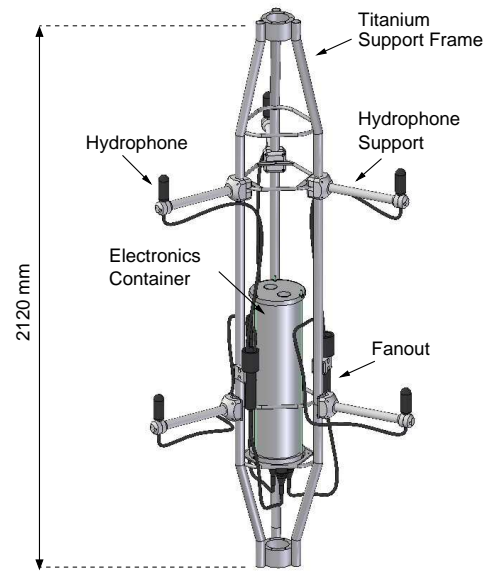


Figure 2. Drawing of a standard acoustic storey, or acoustic cluster, with hydrophones.

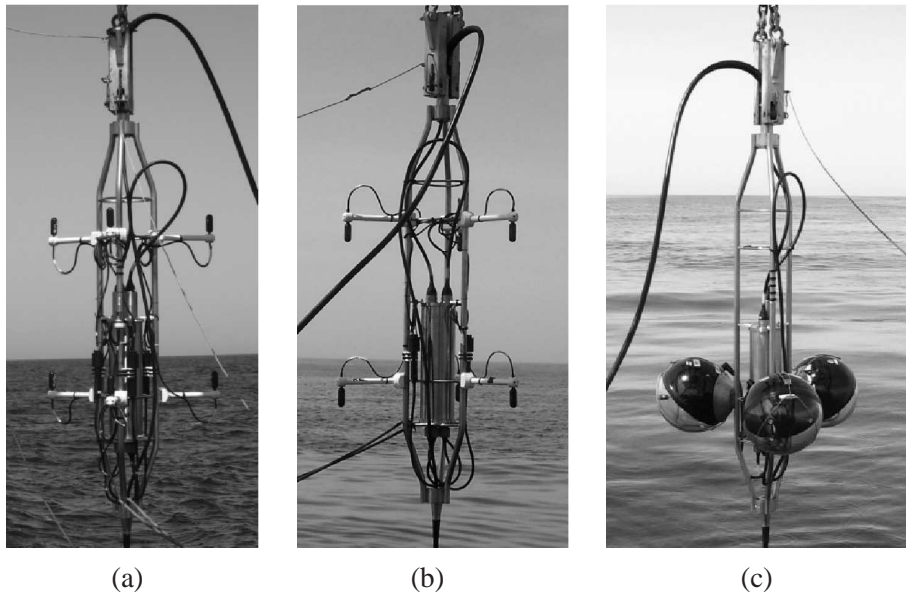


Figure 3. Photographs of three different storeys of the AMADEUS system during their deployment: (a) A standard storey, equipped with hydrophones pointing up; (b) the central acoustic storey on Line 12 with the hydrophones pointing down; (c) the lowermost acoustic storey on Line 12 equipped with Acoustic Modules.

141 2.3 Design Principles

142 A fundamental design guideline for the AMADEUS system has been to use existing
 143 ANTARES hardware and software as much as possible. This eases the operation of
 144 the system within the environment of the ANTARES neutrino telescope; at the

145 same time, the design efforts were kept to a minimum and new quality assurance
146 and control measures had to be introduced only for the additional components.
147 These were subjected to intensive testing procedures, in particular in view of the
148 hostile environment due to the high water pressure of up to 240 bar and the salinity
149 of the water.

150 In order to integrate the AMADEUS system into the ANTARES neutrino telescope,
151 design and development efforts in the following basic areas were necessary:

- 152 • The development of acoustic sensing devices that replace the Optical Modules
153 of standard ANTARES storeys and of the cables to route the signals into the
154 electronics container;
- 155 • The development of an off-shore acoustic digitisation and pre-processing board;
- 156 • The setup of an on-shore server cluster for the online processing of the acoustic
157 data and the development of the online software;
- 158 • The development of offline reconstruction and simulation software.

159 Six acoustic sensors per storey were implemented. This number was the maximum
160 compatible with the design of the LCM and the bandwidth of data transmission
161 to shore. Furthermore, the acoustic storeys were designed such that their size did
162 not exceed the size of the standard ANTARES storeys in radial dimension, hence
163 assuring compatibility with the deployment procedure of the ANTARES lines.

164 2.4 The AMADEUS-0 Test Apparatus

165 In March 2005, a full-scale mechanical prototype line for the ANTARES detector
166 was deployed and subsequently recovered [16]. This line, dubbed *Line 0*, contained
167 no photomultipliers and no readout electronics. Instead, an autonomous data log-
168 ging system and shore-based optical time-domain reflectometry were used to record
169 the status of the setup.

170 Line 0 provided a well-suited environment to study the properties of the acoustic
171 sensors in situ at a time when the readout electronics for AMADEUS was still in
172 the planning phase and the piezo-preamplifier setup in the design phase. For this
173 purpose, an autonomous system within a standard LCM container, the *AMADEUS-*
174 *0* device, was integrated into Line 0. It recorded acoustic signals at the ANTARES
175 site using five piezo sensors with custom-designed preamplifiers with an overall
176 sensitivity of about -120 dB re $1\text{V}/\mu\text{Pa}$ in the range from 5 to 50 kHz, glued to
177 the inside of the LCM container. A battery-powered readout and data logging sys-
178 tem was devised and implemented using commercially available components. The
179 system was further equipped with a timing mechanism to record data over two
180 pre-defined periods: The first one lasted for about 10 hours and included the de-
181 ployment of the line. During this period, a total of 2:45 hours of data were recorded
182 over several intervals. In the second period, with the line installed on the sea floor,

183 1:45 hours of data were taken over a period of 3:30 hours until the battery power
184 was exhausted.

185 The analysis of the data [17] provided valuable information for the design of the
186 AMADEUS system. In particular, the level of the recorded noise allowed for tun-
187 ing the sensitivity and frequency response of the preamplifiers and amplifiers. A
188 filtered amplitude distribution is shown in Figure 4, where signals saturating the
189 readout electronics have been removed. The gaussian fit shown in the figure is a
190 measure of the combined ambient noise of the deep sea and inherent noise of the
191 system, while the excess of data is due to transient signals. This shows that the sen-
192 sitivity of the system is well matched to record background noise while at the same
193 time allowing for a wide dynamic range of transient signals. A comparable overall
194 sensitivity was hence chosen for the AMADEUS setup. The design of the com-
195 mercial readout electronics proved to be not suitable in terms of long-term stability
196 and the response to signals that saturated the readout electronics. This experience
197 was returned to the design of the AMADEUS readout electronics, which will be
198 described in Section 3.4.

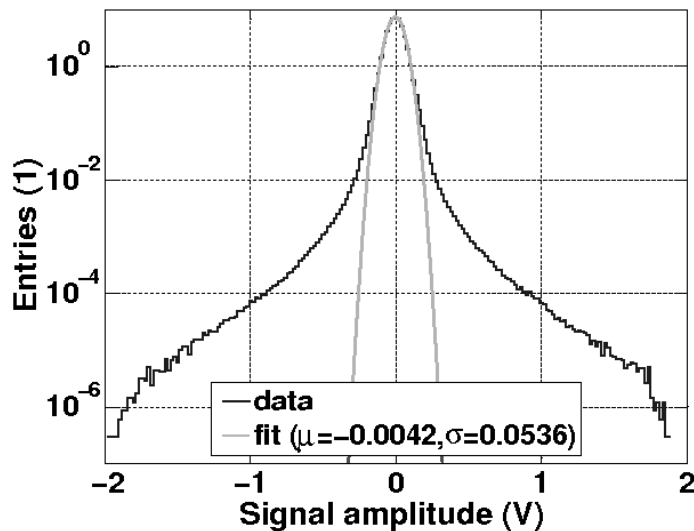


Figure 4. Normalised distribution of signal amplitudes for all data recorded with the AMADEUS-0 device. High amplitude (>2 V) signals, saturating the readout electronics, have been removed. A gaussian fit to the data yields mean μ and standard deviation σ .

199 3 System Components

200 3.1 The Acoustic Sensors

201 The fundamental components of both the hydrophones and the AMs, collectively
202 referred to as acoustic sensors, are piezo-electrical ceramic elements, converting

203 pressure waves into voltage signals [18], and preamplifiers. In this subsection, the
204 hydrophones, the AM sensors, and the calibration of their sensitivity will be dis-
205 cussed.

206 3.1.1 *Hydrophones*

207 A schematic drawing of an ECAP hydrophone is shown in Figure 5. For these
208 hydrophones⁷, two-stage preamplifiers were used: adapted to the capacitive nature
209 of the piezo elements and the low induced voltages, the first preamplifier stage is
210 charge integrating while the second one is amplifying the output voltage of the first
211 stage. The shape of the ceramics is that of a hollow cylinder.

212 Due to hardware constraints of the electronics container, the only voltage avail-
213 able for the operation of the preamplifiers was 6.0 V. In order to minimise elec-
214 tronic noise, the preamplifiers were designed for that voltage rather than employing
215 DC/DC converters to obtain the 12.0 V supply typically used.

216 The piezo elements and preamplifiers of the hydrophones are coated in polyurethane.
217 Plastic endcaps prevent the material from pouring into the hollow part of the piezo
218 cylinder during the moulding procedure. The ECAP as well as the HTI hydrophones
219 have a diameter of 38 mm and a length (from the cable junction to the opposite end)
220 of 102 mm.

221 The equivalent inherent noise level in the frequency range from 1 to 50 kHz is about
222 13 mPa for the ECAP hydrophones and about 5.4 mPa for the HTI hydrophones.
223 This compares to 6.2 mPa of the lowest expected ambient noise level in the same
224 frequency band for a completely calm sea [19], referred to as *sea state 0* [20].

225 At the ANTARES site, the hydrophones are subject to an external pressure of 210
226 to 240 bar, depending on the depth at which they are installed. Prior to deployment,
227 each hydrophone was pressure-tested in accordance with the standard ANTARES
228 procedure, i.e. the pressure was ramped up to 310 bar at 12 bar per minute, held
229 there for two hours and then ramped down again at 12 bar per minute.

230 3.1.2 *Acoustic Modules*

231 For the AMs, the same preamplifiers are used as for the ECAP hydrophones. The
232 piezo elements have the same outer diameter but are solid cylinders in case of the
233 AMs. Two sensors are glued to the inside of each sphere. This design was motivated
234 by the idea to operate the piezo elements at low pressure and also to investigate an
235 option for acoustic sensing that can be integrated together with a PMT in the same

⁷ For the commercial hydrophones, details were not disclosed by the manufacturer, but the main design is similar to the one described here.

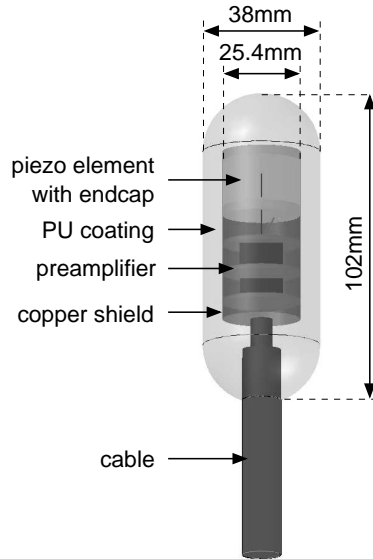


Figure 5. Schematic drawing of an ECAP hydrophone. Piezo element and preamplifier (consisting of three circular circuit boards, interconnected by pin connectors) are moulded into polyurethane (PU).

236 glass sphere. In order to assure a good acoustic coupling, the space between the
 237 curved sphere and the flat end of the piezo sensor of the AMs was filled with epoxy.
 238 A photograph of an Acoustic Module and a schematic drawing of the sensors glued
 239 to the inside of the glass sphere are shown in Figures 6(a) and 6(b), respectively.

240 In order to obtain a 2π azimuthal coverage, the six sensors are distributed over the
 241 three AMs of the storey within the horizontal plane defined by the three centres of
 242 the spheres as shown in Figure 6(c). The spheres have outer diameters of 432 mm.

243 3.1.3 Calibration

244 All sensors are tuned to have a low noise level and to be sensitive over the fre-
 245 quency range from 1 to 50 kHz with a typical sensitivity around -145 dB re $1\text{V}/\mu\text{Pa}$
 246 (including preamplifier). The sensitivities of all sensors as a function of frequency,
 247 polar angle and azimuthal angle were measured before deployment in a water tank,
 248 using a calibrated emitter [21]. The analysis was restricted to frequencies above
 249 10 kHz. Towards lower frequencies, measurements become increasingly less sig-
 250 nificant. This is due to the quadratic frequency dependence of the emitter's transmit
 251 voltage response and to the increasingly adverse effect of reflections for increasing
 252 wavelengths. In accordance with the expected behaviour of the piezo elements, the
 253 sensitivity is assumed to be constant below 10 kHz.

254 The sensitivity of one of the commercial hydrophones is shown in Figure 7 as a
 255 function of frequency for different polar angles. For frequencies below 50 kHz,
 256 the sensitivity decreases once the polar angle approaches 180° , which defines the

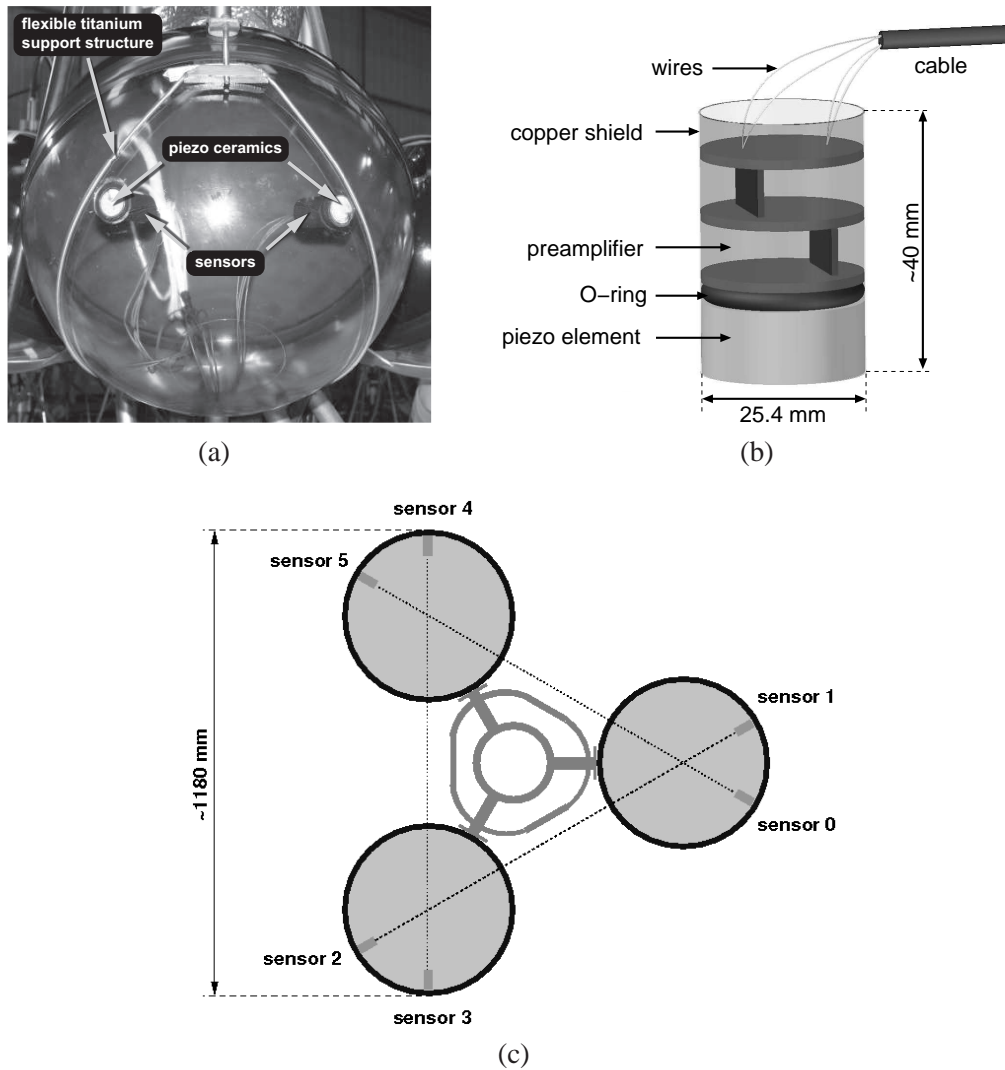


Figure 6. (a) Photograph of an Acoustic Module (AM) before deployment; (b) schematic drawing of an AM sensor; (c) horizontal cross-section of an acoustic storey holding Acoustic Modules in the plane of the sensors. The dotted lines are collinear with the longitudinal axes of the sensors and indicate the arrangement of the sensor within the storey. The lines intersect at angles of 60° at the centres of the glass spheres.

257 direction at which the cable is attached to the hydrophone. The beginning of this
 258 trend can be seen for the polar angle of 150° .

259 The sensitivity as a function of the azimuthal angle for a given frequency is es-
 260 sentially flat at the 3 dB level for all hydrophones. The sensitivity as a function
 261 of polar angle and frequency shows deviations of less than 2 dB between different
 262 HTI hydrophones in the frequency range from 10 to 50 kHz. The deviations for the
 263 hydrophones produced at ECAP are at a level of 3 to 4 dB. The sensitivity of an
 264 ECAP hydrophone is shown in Figure 8. Compared to the HTI hydrophones, the
 265 sensitivity in the frequency range from 10 to 50 kHz is higher but less uniform, both
 266 as a function of frequency and as a function of polar angle.

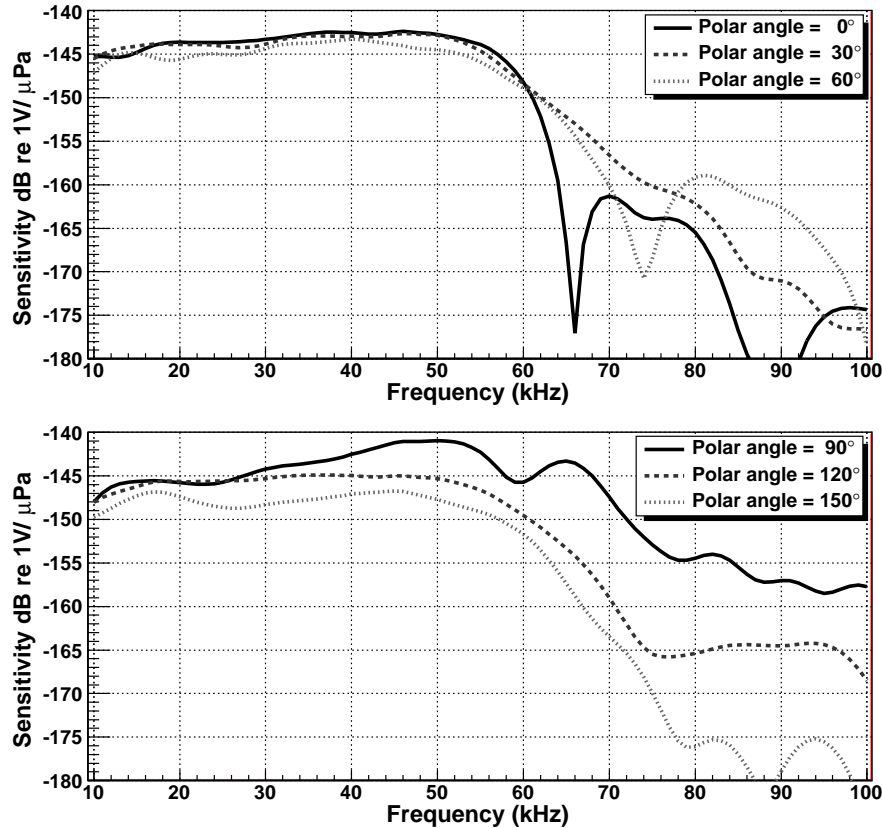


Figure 7. Typical sensitivity of an HTI hydrophone as a function of frequency for different polar angles, averaged over the azimuthal angle. Systematic uncertainties below 50 kHz are 2 to 3 dB.

267 As a consequence of their design, the solid angle over which the sensors of the
 268 AMs are sensitive is smaller compared to the hydrophones. Furthermore, reflections
 269 and resonances within the glass sphere affect the signal shape and frequency
 270 dependence, making laboratory measurements more difficult to interpret. The calibration
 271 was performed by varying the position of the emitter along a half circle,
 272 such that each emitter position has the same distance to the piezo element. Angles
 273 were then given by the position of the emitter along the half circle with respect to
 274 the longitudinal axis of the piezo sensor, which defined the angle of 0° . Results are
 275 shown in Figure 9. The higher sensitivity compared to the ECAP hydrophones is
 276 due to the different piezo element that is used and the acoustic coupling between
 277 water, the glass sphere and the piezo sensor.

278 All sensitivity measurements were done at normal pressure. A verification with an
 279 in situ calibration has not yet been carried out at the time of the writing of this
 280 paper.

281 For the calibration that was describe above, gaussian signals were emitted which in
 282 the frequency domain cover the range of the calibration. In addition, the response
 283 of the sensors to bipolar pulses was recorded. This is shown in Figure 10. The

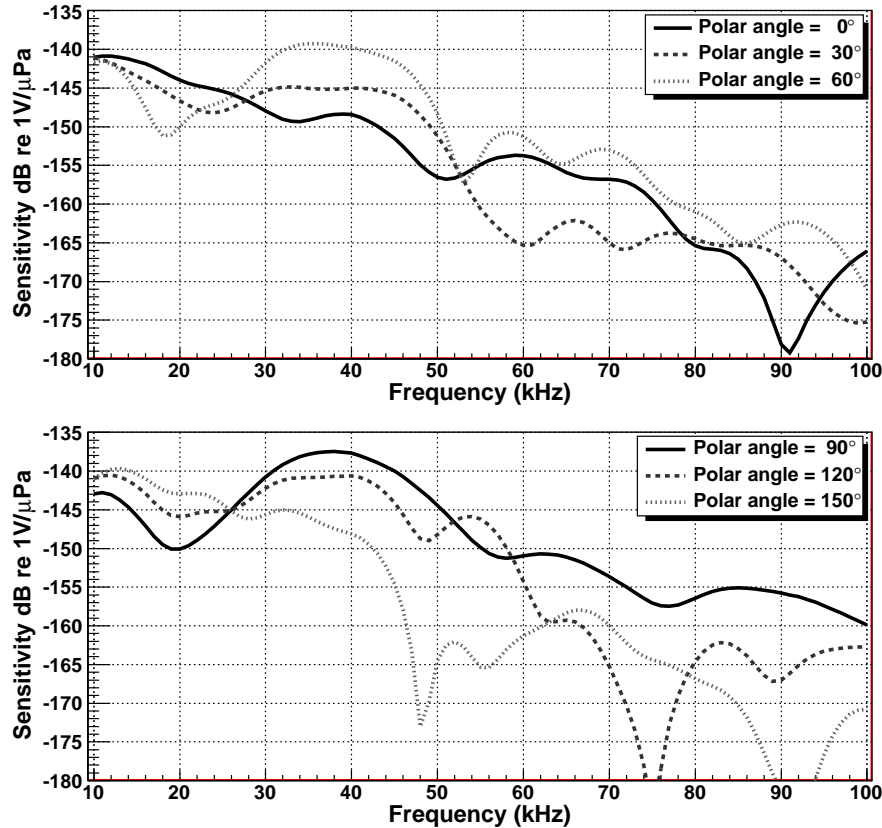


Figure 8. Typical sensitivity of an ECAP hydrophone as a function of frequency for different polar angles, averaged over the azimuthal angle. Systematic uncertainties below 50 kHz are 2 to 3 dB.

284 agreement between the different sensor types is quite good. The asymmetry of the
 285 input pulse, i.e. the ratio of the pulse heights at the positive and negative peaks, can
 286 be seen to be diminished in the response of the sensors. This is due to the excitation
 287 of oscillations of the piezo elements.

288 3.2 Cables and Connectors

289 Each electronics container is equipped with three 12-pin SubConn connector sock-
 290 ets⁸. In order to connect two hydrophones to each of the three sockets, special
 291 *fanout cables* were produced (see Figure 2). To the electronics container end of the
 292 cable, the same mating connector plugs are used as for the Optical Modules. At the
 293 other end of the cable, a bulkhead connector AWQ-4/24 of the ALL-WET split series
 294 by Seacon⁹ was moulded, which fans out into six wedge-shaped sectors. Each
 295 sector has a 4-pin connector socket, serving the four leads for individual power
 296 supply and differential signal readout of the hydrophones. Each of the mating 4-pin

⁸ MacArtney Underwater Technology group, <http://www.subconn.com/>

⁹ Seacon (Europe) LTD, Great Yarmouth, Norfolk, UK, <http://www.seaconeurope.com/>

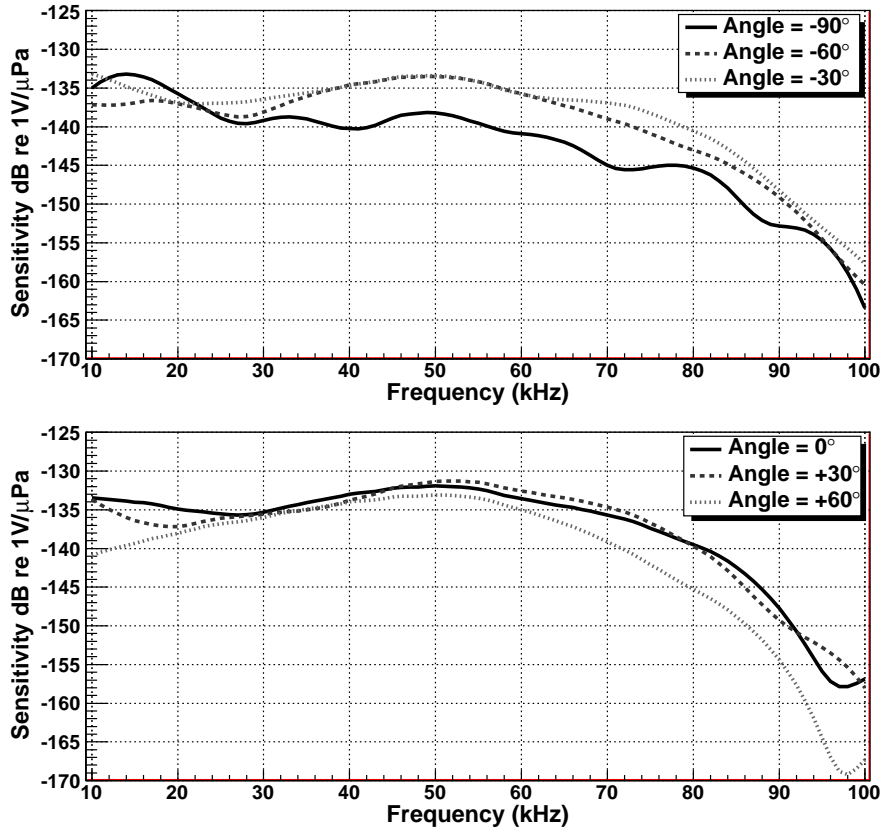


Figure 9. Sensitivity of an AM sensor as a function of frequency for different angles with respect to the longitudinal axis of the sensor. Systematic uncertainties below 50 kHz are 2 to 3 dB.

297 connectors is moulded to a neoprene cable with the hydrophone at its other end.
 298 The remaining four sectors of the bulkhead connector are sealed with blind plugs.

299 The standard cables used in the ANTARES detector between the electronics con-
 300 tainer and the Optical Modules are also used to connect the AMs. The LCMs inte-
 301 grated into storeys with AMs and with hydrophones are interchangeable. All con-
 302 nections and cables within AMADEUS are functioning as expected.

303 3.3 Off-Shore Electronics

304 In the ANTARES data acquisition (DAQ) scheme [22], the digitisation is done
 305 within the off-shore electronics container (see Section 2). Each LCM contains a
 306 backplane that is equipped with sockets for the electronics cards and provides them
 307 with power and data lines. A standard LCM for processing the data from PMTs
 308 contains the following electronics boards:

- 309 • Three *ARS motherboards*, each comprising two Analogue Ring Sampler (ARS)
 310 ASICs, for conditioning and digitisation of the analogue signals from the PMTs [23];

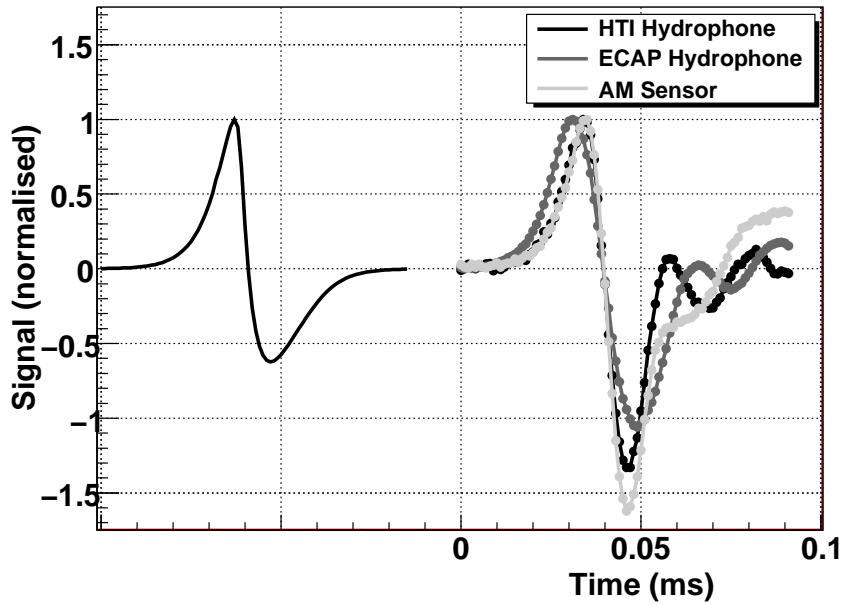


Figure 10. Comparison of the response of different acoustic sensor types to a bipolar pulse. The emitted signal is shown on the left. The response of the hydrophones was measured for a polar angle of 90° , the response of the AM sensor for an angle of 0° . The first peak of each pulse (including the emitted one) was normalised to 1 and the time axis of each received signal was adjusted such that the times of the zero crossings coincide. The time offset between emitted and received pulses in the depiction is arbitrary.

- 311 • A *DAQ board*, which reads out the ARS motherboards and handles the commu-
312 nication to shore via TCP/IP;
- 313 • A *Clock board* that provides the timing signals to correlate measurements per-
314 formed in different storeys (see Subsection 3.6);
- 315 • A *Compass board* to measure the tilt and the heading of the storey.

316 The transmission of data to shore is done through a *Master LCM (MLCM)* which—
317 in addition to the components of an LCM described above—contains an ethernet
318 switch and additional boards for handling incoming and outgoing fibre-based op-
319 tical data transmission. Up to five storeys form a *sector*, in which the individual
320 LCMs transmit the data to the MLCM.

321 For the digitisation of the acoustic signals and for feeding them into the ANTARES
322 data stream, the *AcouADC board* was designed. These boards are pin-compatible
323 with the ARS motherboards and replace them in the acoustic storeys. Figure 11
324 shows the fully equipped LCM of an acoustic storey.

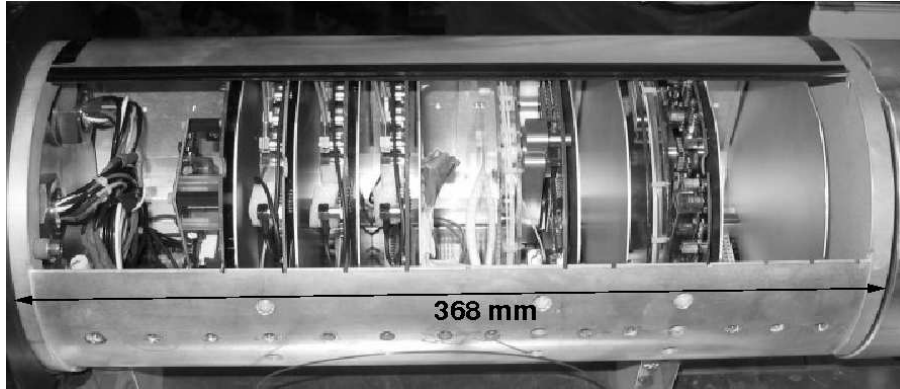


Figure 11. An LCM during assembly, equipped with AcouADC boards before insertion into the titanium container. The sockets for external connection (not visible in this picture) are attached to the lid of the container on the left-hand side of the photograph. From left to right, the following boards are installed: a Compass board; three AcouADC boards; a DAQ board; a Clock board.

3.4 The AcouADC Board

Each AcouADC board serves two acoustic sensors and has the following major tasks:

- Pre-processing of the analogue signals (impedance matching, application of an anti-alias filter, selectable gain adjustment);
- Digitisation of the analogue signals and preparation of the digitised data stream for transmission to the DAQ board;
- Provision of stable low-noise voltage (6.0 V) for power supply of the acoustic sensors;
- Provision of an interface to the on-shore slow control software (see Subsection 3.5).

A photograph and a block diagram of an AcouADC board are shown in Figures 12 and 13, respectively. The board consists of an analogue and a digital signal processing part. Each board processes the differential voltage signals from two acoustic sensors, referred to as “Sig 0” and “Sig 1” in the diagram. The two signals are processed independently and in parallel for the complete (analogue and digital) data processing chain.

A main design criterion for the board was a low inherent noise level, so that even for sea state 0 no significant contribution to the recorded signal originates from the electronics of the board. To protect the analogue parts from potential electromagnetic interference, they are shielded by metal covers. Tests of the electromagnetic compatibility (EMC) of the board have shown that this design is not significantly affected by electromagnetic noise even for conditions that are far more unfavourable than those present in situ [19].

349 The two 6.0 V power supply lines on each AcouADC board (connectors labelled
350 “Pow 0” and “Pow 1” in Figure 13) are protected by resettable fuses against short
351 circuits that could be produced by the sensors due to water ingress. In addition,
352 each voltage line can be individually switched on or off.

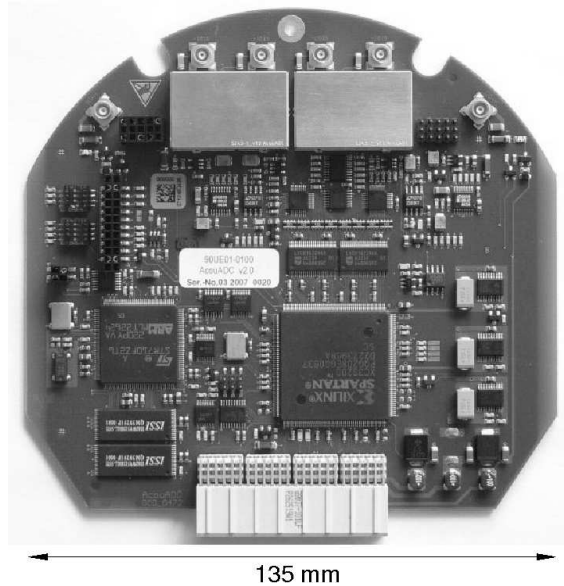


Figure 12. Photograph of an AcouADC board. The four connectors for the two differential input signals are located at the top, the analogue signal processing electronics is covered by metal shields.

353 3.4.1 Analogue Signal Processing

354 The analogue signal is amplified in two stages. The first stage applies a coarse gain
355 with nominal amplification factors of 1, 10 or 100. It is implemented as a differential
356 amplifier with single-ended output, referenced to 2.5 V. The gain factor 1 is used
357 for recording dedicated runs with large signal amplitudes, e.g. from the emitters of
358 the ANTARES acoustic positioning system (see Subsection 2.1), whereas the factor
359 of 100 was only foreseen for the case that the sensitivity of the hydrophones would
360 degrade after deployment.

361 The second amplification stage, the fine gain, is intended to adjust the gains of dif-
362 ferent types of hydrophones. It is a non-inverting amplification with single ended
363 output and a reference voltage of 2.5 V. Gain factors of 1.00, 1.78, 3.16, and 5.62
364 (corresponding to 0, 5, 10, and 15 dB, respectively) are selectable by switching be-
365 tween four appropriate resistors in the feedback loop of the operational amplifier.
366 Combining the two stages, the gain factor can be set to one of 12 values between 1
367 and 562. The standard setting is an overall gain factor of 10, yielding the approxi-
368 mimate sensitivity of -125 dB re $1\text{V}/\mu\text{Pa}$.

369 After amplification, the signal is coupled into a linear-phase 10th-order anti-alias

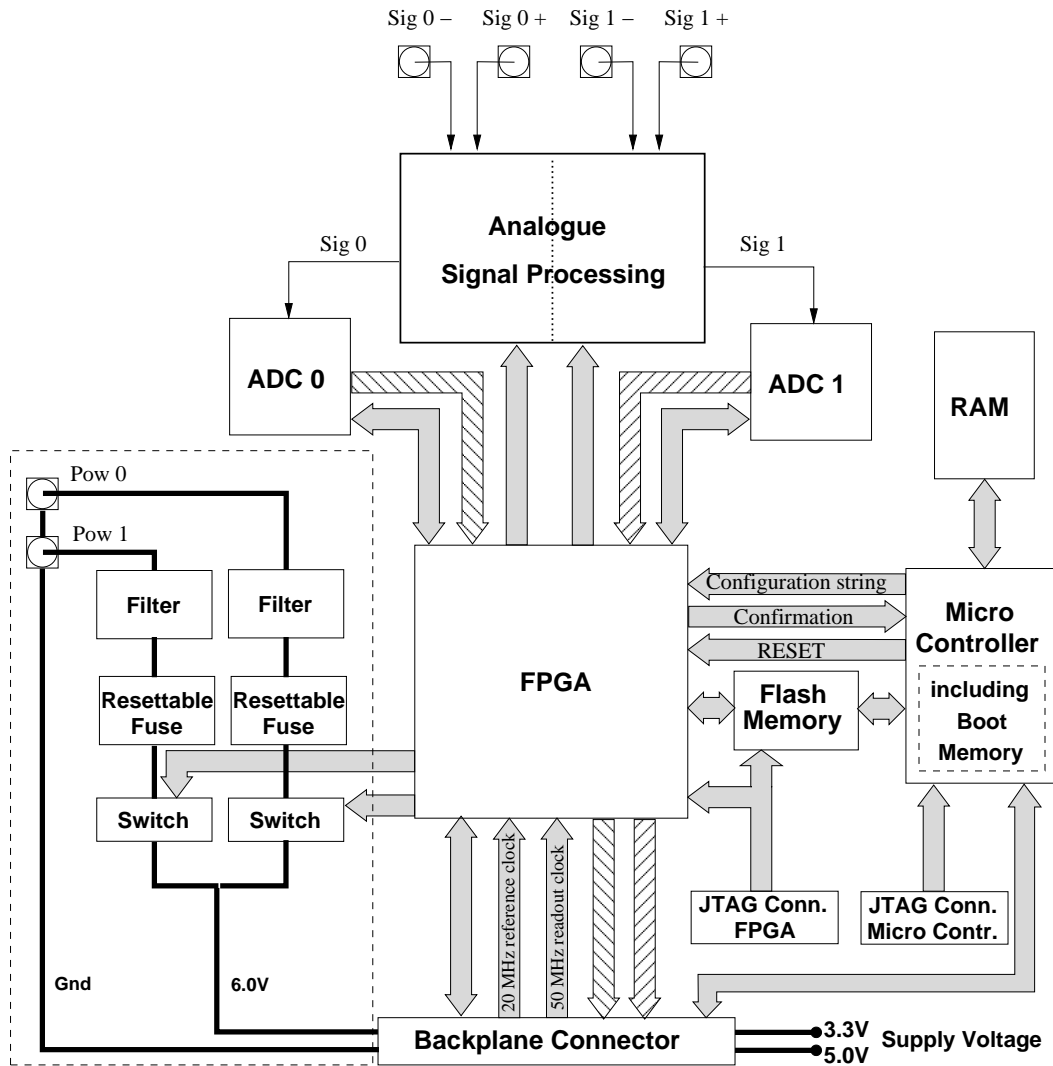


Figure 13. Block diagram of the AcouADC board. The flow of the analogue sensor signals entering from the connectors (squares with inserted circles) at the top of the figure is indicated by thin arrows. Hatched arrows denote the flow of the digitised data further downstream. General communication connections are shown as shaded arrows. The components relevant for the power supply of the hydrophones are shown in the left part. Voltage supply lines are shown as thick lines, the dashed box indicates the circuitry for the power supply of the acoustic sensors.

370 filter¹⁰ with a root-raised cosine amplitude response and a 3 dB point at a frequency
 371 of 128 kHz. In low-power mode, the filter output range is about 3.9 V. The output is
 372 referenced to 2.0 V and fed into a 16-bit analogue-to-digital converter (ADC) that
 373 will be described below. Accordingly, the ADC reference voltage is set to 2.0 V,
 374 implying that the digital output of zero corresponds to this analogue value. The
 375 input range of the ADC is 0.0 to 4.0 V.

376 The three analogue stages (coarse and fine amplification and anti-alias filtering)

¹⁰ Filter LTC1569-7 from Linear Technology, <http://www.linear.com/>

377 and the ADC are decoupled by appropriate capacitors. Furthermore, several RCL
378 elements within the analogue signal chain form an additional band-pass filter. Its
379 low-frequency 3 dB point is at about 3 kHz and cuts into the trailing edge of the low-
380 frequency noise of the deep-sea acoustic background [24], protecting the system
381 from saturation. The high-frequency 3 dB point is above 1 MHz and was introduced
382 to comply with the input requirements of active components of the circuitry.

383 3.4.2 *Digital Signal Processing*

384 The digital part of the AcouADC board digitises the acoustic signals and processes
385 the digitised data. It is flexible due to the use of a micro controller (μC)¹¹ and
386 a field programmable gate array (FPGA)¹² as data processor. All communication
387 with the shore is done via the DAQ board; the μC handles the slow control (see
388 Subsection 3.5) and the FPGA the data transfer. The μC is accessed from the on-
389 shore control software and is used to adjust settings of the analogue part and the
390 data processing. It can also be used to update the firmware of the FPGA. This
391 firmware is stored in a flash memory and loaded after a reset of the FPGA. In
392 situ, this reset is asserted from the μC . If a firmware update is performed, the μC
393 first loads the code from the shore into the random access memory (RAM). Once
394 the integrity of the code has been confirmed by means of a checksum, the code
395 is transmitted into the flash memory. In order to avoid the potential risk that a
396 software error renders the μC inaccessible, its boot memory can only be changed
397 in the laboratory. For testing and programming in the laboratory, JTAG¹³ is used
398 to access the FPGA, the μC , and the flash memory.

399 For each of the two input channels, the digitisation is done at 500 kSps (kilosam-
400 ples per second) by one 16-bit successive approximation ADC¹⁴ with output range
401 from -32768 to $+32767$ counts. The two ADCs are read out in parallel by the
402 FPGA and further formatted for transmission to the DAQ board.

403 ADCs commonly show relatively high deviations from a linear behaviour near the
404 zero value of their digital output. The size of this effect depends on the circuitry
405 into which the ADC is embedded. For the prototypes of the AcouADC boards, this
406 effect proved to be fairly pronounced. For this reason, the reference voltage of the
407 anti-alias filter output can be switched from its standard value of 2.0 V to 1.0 V,
408 thereby moving the centre of the acoustic noise distribution away from the digital
409 value of zero. This leads to an asymmetry of the recordable range for positive and
410 negative amplitudes of acoustic signals, effectively reducing the dynamic range

¹¹ STR710 from STMicroelectronics, <http://www.st.com/>

¹² Spartan-3 XC3S200 from Xilinx, <http://www.xilinx.com/>

¹³ The IEEE standard 1149.1 “Test Access Port and Boundary-Scan Architecture” is commonly referred to as JTAG, the acronym for Joint Test Action Group. It defines an interface to individual components on a circuit board.

¹⁴ ADS8323 from Analog Devices, <http://www.analog.com/>

411 by a factor of 2 if one requires both positive and negative amplitudes to be fully
412 recorded. For standard data taking, this is not desirable whereas the non-linearities
413 of the ADCs proved to be unproblematic. Therefore, the reference voltage of the
414 anti-alias filter output is set to 1.0 V only for special measurements.

415 In standard mode, the sampling rate is reduced to 250 kSps in the FPGA, corre-
416 sponding to a downsampling by a factor of 2 (DS2). Currently implemented op-
417 tions are DS1 (i.e. no downsampling), DS2, and DS4, which can be selected from
418 the shore. For each downsampling factor an adapted digital anti-alias filter, compli-
419 ant with the Nyquist-Shannon sampling theorem, is implemented in the FPGA as a
420 finite impulse response (FIR) filter with a length of 128 data points. For DS2, the
421 frequency spectrum between the 3 dB points at 2.8 and 108.8 kHz passes the filter.

422 3.4.3 System Characteristics

423 The complex response function of the AcouADC board (i.e. amplitude and phase)
424 was measured in the laboratory prior to deployment for each board and a parametri-
425 sation of the function was derived [19]. Figure 14 shows the frequency response of
426 the AcouADC board. The measurement was done by feeding gaussian white noise
427 into the system and analysing the digital output recorded by the board. Without
428 downsampling (DS1), the rolloff at high frequencies is governed by the analogue
429 anti-alias filter. For DS2 and DS4, the digital FIR filters are responsible for the be-
430 haviour at high frequencies. At low frequencies, the effect of the band-pass filter
431 described above can be seen. Figure 14 furthermore demonstrates that within each
432 passband, the filter response is essentially flat. The comparison of the recorded data
433 with the parametrisation shows excellent agreement.

434 The parametrisation of the response function allows to calculate the response of the
435 system to any input pulse and vice versa the reconstruction of the original shape of
436 any recorded pulse. Figure 15 shows a comparison of the measured and calculated
437 response of the analogue signal processing part of the AcouADC board to a generic
438 bipolar input pulse as it would be expected from a neutrino-induced cascade (see
439 Section 1). The digital FIR filter introduces an additional time offset of 128 μ s of
440 the digitised data for DS2 and DS4.

441 The ADCs of the AcouADC board were investigated in detail [19]. For each indi-
442 vidual ADC, the transfer curve from input voltage to ADC counts was measured
443 and distortions from the ideal linear behaviour quantified in terms of the differ-
444 ential nonlinearity (DNL) and integral nonlinearity (INL). The distribution of the
445 DNL values for all bins of all calibrated signal channels shows negligible deviations
446 from the ideal situation (i.e. a peak at zero) with a mean of -0.02 ADC counts and
447 a standard deviation of 0.06 ADC counts, corresponding to 3.4 μ V. The values of
448 the INL of the ADCs stay within 50 ADC counts for all signal channels over the
449 full input range, corresponding to ± 3.1 mV.

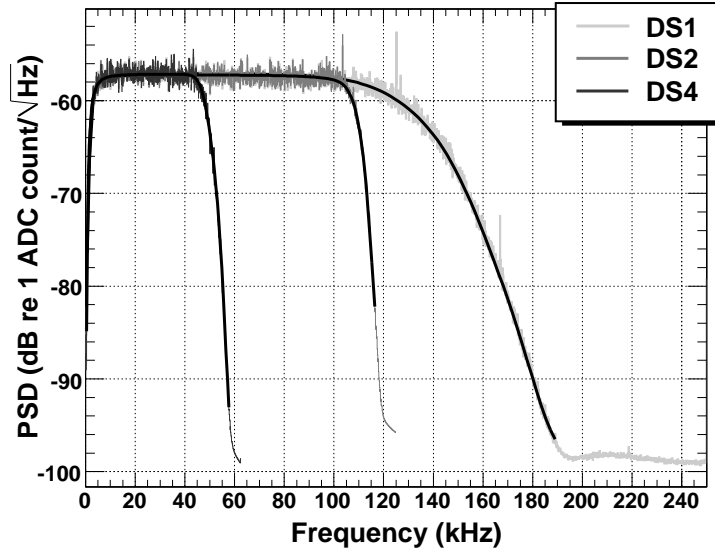


Figure 14. The AcouADC board filter response, characterised by a power spectral density (PSD) as a function of frequency, measured for the three different downsampling factors. For each of the three measurements, the parametrisation is shown as a black line.

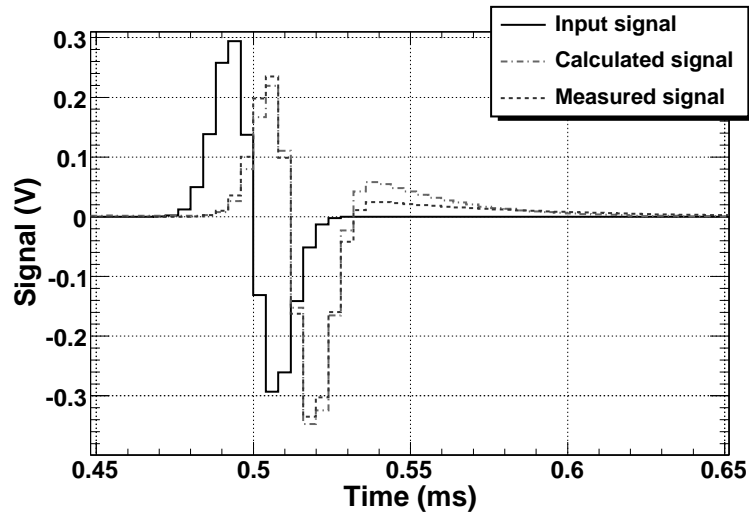


Figure 15. The response of the analogue part of an AcouADC board to a bipolar input pulse. Shown are the measured output signal and the output signal calculated from the parametrised response function. The measured output signal was obtained with an oscilloscope at the input of the ADC. The measurement was done for a nominal gain factor of 1.

450 The spurious-free dynamic range (SFDR) of an ADC is a measure of its dynamic
 451 range. Using a sinusoidal input signal, the average SFDR of the ADCs of all boards
 452 in AMADEUS was measured to be 59.9 ± 1.1 dB, meaning that harmonics of the
 453 sine wave distorting the output signal are suppressed by 3 orders of magnitude in
 454 the amplitude. Hence, a clear determination of the frequency is possible even for
 455 saturated signals, for which the harmonic components are enhanced.

456 The 12 gain factors for each channel were calibrated and the correction factor for
457 gain 1 was measured to be 1.05 ± 0.01 . The gain factors of the other 11 settings were
458 measured with respect to this value and were found to deviate from the nominal
459 factors by about 10% at maximum.

460 The inherent noise of the electronics (output for open signal input) and the cross-
461 talk between the two signal channels of an AcouADC board were measured to be
462 negligible in comparison with the inherent noise of the acoustic sensors.

463 3.5 *Slow Control System*

464 The ANTARES slow control (SC) system has two main tasks. It provides the off-
465 shore components with initialisation and configuration parameters and it regularly
466 monitors whether the operational parameters are within their specified ranges. In
467 addition, the readout of some instruments for environmental monitoring [25], per-
468 formed at intervals of a few minutes, is polled and sent through the SC interface.

469 For the AMADEUS system, the following parameters can be set from shore via the
470 SC system for each acoustic channel individually: one of the 12 values for the gain;
471 downsampling factors of 1, 2, or 4 (or no data transmission from the AcouADC
472 board); power supply for the acoustic sensor on or off; reference voltage of the
473 analogue signal fed into the ADC 2.0 V or 1.0 V.

474 To monitor the environment within each LCM container, a humidity sensor and
475 temperature sensors on several boards are installed. One temperature sensor is
476 placed on each AcouADC board. Values read out by the SC system are stored in an
477 Oracle[®] database that is centrally used by ANTARES.

478 3.6 *Data Acquisition and Clock System*

479 AMADEUS uses the same DAQ system and follows the same “all data to shore”
480 strategy [22] as the ANTARES neutrino telescope, i.e. all digitised data are trans-
481 mitted to shore via optical fibres using the TCP/IP protocol. The data stream from
482 the sender DAQ board is tagged with the IP address of the receiving on-shore server.
483 In the control room, the acoustic data are routed to a dedicated computer cluster
484 by using the transmitted IP address. The ANTARES clock system operates sepa-
485 rately from the DAQ system, using a different set of optical fibres to synchronise
486 data from different storeys. The system provides a highly stable 20 MHz synchroni-
487 sation signal, corresponding to a resolution of 50 ns¹⁵, which is generated by a

¹⁵ The much higher precision that is required for the synchronisation of the optical signals from the PMTs is provided by a 256-fold subdivision of the 20 MHz signal in the ARS

488 custom-designed system at the ANTARES control room. The synchronisation of
489 this internal clock with the UTC¹⁶ of the GPS system is established with a preci-
490 sion of 100 ns.

491 The synchronisation signal is broadcast to the off-shore clock boards and from there
492 transmitted further to the FPGA of the AcouADC board. Based on this signal, the
493 data packages sent from the AcouADC board to shore via the DAQ board receive
494 a timestamp which allows for correlating the data from different storeys. The 50 ns
495 resolution of the timestamp by far exceeds the requirements given by the standard
496 sampling time of 4 μ s corresponding to DS2. Differences in the signal transit times
497 between the shore station and the individual storeys are also smaller than 4 μ s and
498 do not need to be corrected for.

499 3.7 On-Shore Data Processing and System Operation

500 The AMADEUS system is operated with its own instance of the standard ANTARES
501 control software called *RunControl* [22]. This is a program with a graphical user
502 interface to control and operate the experiment. It is JavaTM-based and reads the
503 configuration of the individual hard- and software components from the ANTARES
504 database, allowing for an easy adaption of individual run parameters for the AMADEUS
505 system. Via the clock system the absolute time of the run start is logged in the
506 database with the aforementioned precision of 100 ns. The end of a run is reached
507 if either the data volume or the duration exceed predefined limits (in which case a
508 new run is started automatically) or the run is stopped by the operator. The data of
509 one AMADEUS run are stored in a single file in *ROOT* format [26]. The typical
510 duration of a run ranges from 2 to 5 hours.

511 For the computing requirements of AMADEUS, a dedicated on-shore computer
512 cluster was installed. It currently consists of four server-class computers, of which
513 two are used for data triggering¹⁷ (equipped with 2 \times dual core 3 GHz Intel Xeon
514 5160 and 2 \times quad core 3 GHz Intel Xeon 5450 processors, respectively). Hence, a
515 total of 12 cores are available to process the data. One of the remaining two com-
516 puters is used to write the data to an internal 550 GB disk array (RAID), while the
517 other is used to operate the RunControl software and other miscellaneous processes
518 and to provide remote access to the system via the Internet.

519 The AMADEUS trigger searches the data by an adjustable software filter; the
520 events thus selected are stored to disk. This way the raw data rate of about 1.5 TB/day
521 is reduced to about 10 GB/day for storage. Currently, three trigger schemes are

motherboards.

¹⁶ Coordinated Universal Time

¹⁷ While this functionality might be more commonly referred to as filtering, it is ANTARES convention to refer to the “on-shore trigger”.

522 in operation [27]: A minimum bias trigger which records data continuously for
523 about 10 s every 60 min, a threshold trigger which is activated when the signal ex-
524 ceeds a predefined amplitude, and a pulse shape recognition trigger. For the latter,
525 a cross-correlation of the signal with a predefined bipolar signal, as expected for a
526 neutrino-induced cascade, is performed. The trigger condition is met if the output
527 of the cross-correlation operation exceeds a predefined threshold. With respect to a
528 matched filter, this implementation reduces the run time complexity while yielding
529 a comparable trigger performance.

530 As discussed in Section 1, for pressure pulses induced by neutrino interactions the
531 amplitude, asymmetry and frequency spectrum depend on the position of the ob-
532 server with respect to the particle cascade. The predefined bipolar signal used for
533 the pulse shape recognition trigger corresponds to the pulse shape expected at a dis-
534 tance of roughly 300 m from the shower centre in the direction perpendicular to the
535 shower axis, i.e. where the maximum signal within the flat volume of sound propa-
536 gation is expected. The cross correlation with pulses whose shape differs from the
537 implemented one changes the peak in the cross correlation output: it is broadened
538 and diminished as compared to the filter response on the predefined signal. This
539 effectively increases the trigger threshold in terms of pressure amplitude for such
540 pulses. As will be described below, the final trigger decision requires coincidences
541 within an acoustic storey, which allows the trigger threshold for the cross correla-
542 tion output of each individual acoustic sensor to be set to a low value. Given that the
543 main purpose of the AMADEUS system is the investigation of background noise,
544 this implementation is very efficient in recording a wide range of bipolar and multi-
545 polar events. Dedicated searches for neutrino signals—which are difficult due to the
546 geometry of the acoustic storeys within the AMADEUS system—are done offline,
547 taking into account the variations of the pulse shapes with distance and direction.

548 Both the threshold and the pulse shape recognition trigger are applied to the indi-
549 vidual sensors and are self-adjusting to the ambient noise, implying that all trigger
550 thresholds are defined in terms of a signal-to-noise ratio. The trigger thresholds
551 are software parameters and therefore can be set at will. The noise level is calcu-
552 lated from and applied to the data of the *frame* that is currently being analysed.
553 A frame denotes the structure in which data are buffered off-shore by the DAQ
554 board before being sent to shore and contains data sampled during an interval of
555 about 105 ms [22]. If one of these two trigger conditions is met, an additional trig-
556 ger condition is imposed, which requires coincidences of a predefined number of
557 acoustic sensors on each storey. The coincidence window is fixed to the length of a
558 frame. Currently, the coincidence trigger requires that the threshold or pulse shape
559 recognition trigger conditions have been met for at least four out of six sensors of
560 a storey.

561 In the ANTARES DAQ system, the frames start at fixed intervals with respect to the
562 run start. Trigger conditions are imposed on temporally corresponding frames from
563 all storeys simultaneously, whereupon the frames are discarded and data not se-

564 lected by the trigger are lost. Processing subsequent frames at the same time is not
565 possible. Given the distances of typically 1 m between sensors within one storey,
566 time delays between signals from a given source are always less than 1 ms. There-
567 fore, the number of sources for which the signals extend over two frames, and hence
568 the coincidence trigger may not be activated, is small. The disadvantage of a large
569 trigger window, the increased probability for random coincidences, leads only to a
570 small increase of the recorded data volume. The coincidence trigger can be option-
571 ally extended to require coincidences between different storeys on the same line.
572 With distances between storeys ranging from about 10 to 100 m (corresponding to
573 delays of the order of 10 to 100 ms) signals originating from above or below are
574 suppressed. This trigger is currently not enabled.

575 The data of all sensors that have fired a coincidence trigger are stored within a com-
576 mon time window that covers all triggered signals. Its minimum length is 1.536 ms
577 for 4 μ s sampling time (corresponding to 384 data samples) and its maximum
578 length corresponds to the length of a frame.

579 The triggers of the AMADEUS system and the main ANTARES optical neutrino
580 telescope are working completely independently. Hence, the search for correlated
581 signals relies on offline analyses.

582 Both the off-shore and on-shore part of the AMADEUS system are scalable, ren-
583 dering it very flexible. The enlargement of the system from three to six acoustic
584 storeys with the commissioning of Line 12 (see Subsection 2.1) was easily im-
585 plemented by increasing the on-shore computing power and updating the control
586 software. In principle, the system could be upgraded to much bigger numbers of
587 acoustic storeys. To reduce the data volume transmitted to shore, it would also be
588 possible to move parts of the trigger algorithms into the FPGA of the AcouADC
589 board.

590 AMADEUS is controlled remotely via the Internet. Data are centrally stored and
591 are remotely available.

592 **4 System Performance**

593 *4.1 General*

594 AMADEUS is continuously operating and taking data with only a few operator
595 interventions per week. The up-time of each sensor is typically better than 80%.
596 Its ability to continuously send unfiltered data, sampled at high frequency, to shore
597 for further analysis renders the AMADEUS system a multipurpose apparatus for
598 neutrino feasibility studies, acoustic positioning and marine research.

599 The concept of acoustic clusters (i.e. the acoustic storeys) is very beneficial for fast
600 online processing. By requiring coincident signals from at least four sensors within
601 a storey, the trigger rate is significantly reduced, improving the purity of the sample
602 selected with the pulse shape recognition trigger.

603 The parallel operation of two separate RunControl programs for AMADEUS and
604 the main ANTARES neutrino telescope, which was originally not foreseen, has
605 proven to be very successful. No interference between the two programs has been
606 observed while the two systems can optimise their detection efficiency and respond
607 to potential problems almost independently. At the same time, both systems profit in
608 the same fashion from developments and improvements of the RunControl software
609 and monitoring tools.

610 The stability of the system response is excellent. This was verified prior to deploy-
611 ment as well as in situ. It was quantified by observing the mean of the ambient noise
612 distribution as a function of time. In situ, the 10 s of continuous data recorded every
613 hour with the minimum bias trigger were used to calculate the mean. The standard
614 deviation of this value for the first year of operation is less than 2×10^{-5} of the full
615 range.

616 All sensor types described in Subsection 2.2 are well suited for the investigation
617 of acoustic particle detection methods. A comparison of the characteristics of the
618 different sensor types will be drawn below.

619 4.2 *Ambient Noise*

620 Studies of the power spectral density of the ambient noise at the ANTARES site
621 have been performed using the minimum bias trigger data. Figure 16 shows the
622 noise levels recorded with representative HTI and ECAP hydrophones and with
623 one AM sensor on Line 12 over several time periods with a combined duration
624 of six months. For each sensor, the power spectral density was calculated for the
625 10 s intervals of continuous data and then for each 1 kHz bin, the median and the
626 0.27% quantile (corresponding to a 3σ deviation from the median) were derived for
627 the complete set of measurements. For each sensor, one can observe a characteris-
628 tic frequency above which the 0.27% quantile of the noise level shows a constant
629 difference to the median. The corresponding frequencies are about 35 kHz, 30 kHz,
630 and 40 kHz for the HTI hydrophones, ECAP hydrophones and AM sensors, respec-
631 tively. For higher frequencies, the noise is dominated by the intrinsic electronics
632 noise, limiting the capability to study the acoustic noise.

633 The noise floor is the lowest for the HTI hydrophones, the difference in the power
634 spectral density to the ECAP hydrophones and AM sensors being 10 to 15 dB.
635 When recording transient signals, the effect on the signal-to-noise ratio is partially
636 compensated by the higher sensitivity of the ECAP hydrophones and the AM sen-

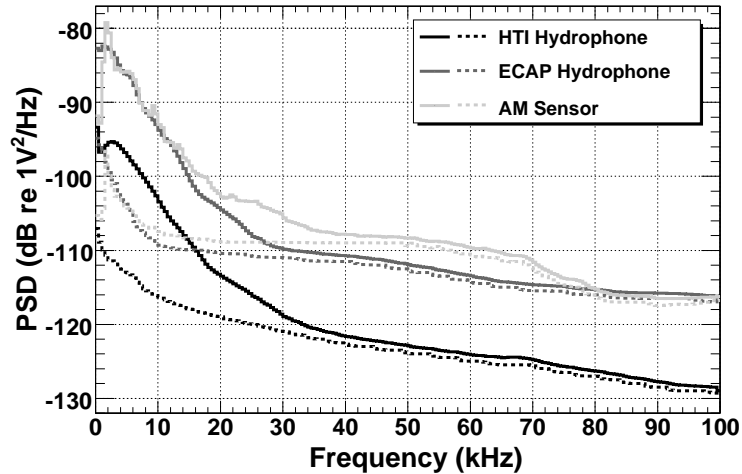


Figure 16. Power spectral density (PSD) of the noise level recorded in situ. Solid lines represent the median, dotted lines the 0.27% quantile (corresponding to a 3σ deviation from the median). The voltage used is the calibrated input voltage of the AcouADC board.

sors. The noise spectrum of the AM sensor displays some structure for frequencies up to about 25 kHz. This is due to coupling of the sensor to the glass spheres. In summary, for studies of the in-situ ambient noise, the HTI hydrophones are the most suited type of sensors.

In Figure 17 a more detailed presentation of the noise data recorded with an HTI hydrophone during the year of 2008 is given. An algorithm to remove strong transient signals (mostly coming from the emitters of the acoustic positioning system) was applied. The relics of such signals and electronics noise show up as spikes between 45 and 75 kHz. The lowest level of recorded noise in situ was confirmed to be consistent with the inherent noise of the system recorded in the laboratory prior to deployment. The observed in-situ noise can be seen to go below the noise level measured in the laboratory for frequencies exceeding 35 kHz. This is due to electronic noise coupling into the system in the laboratory that is absent in the deep sea.

The overall noise levels (i.e. the RMS of the signal amplitudes in each 10 s sample) recorded at the same time with any two active sensors of the same type are correlated at a level above 90%. This shows that the recorded data are indeed representative of the ambient conditions and not determined by the inherent noise of the system.

4.3 Transient Signals and Dynamic Range

The signals recorded with the three different types of acoustic sensors on Line 12 for a common source is shown in Figure 18. The signals were recorded in May

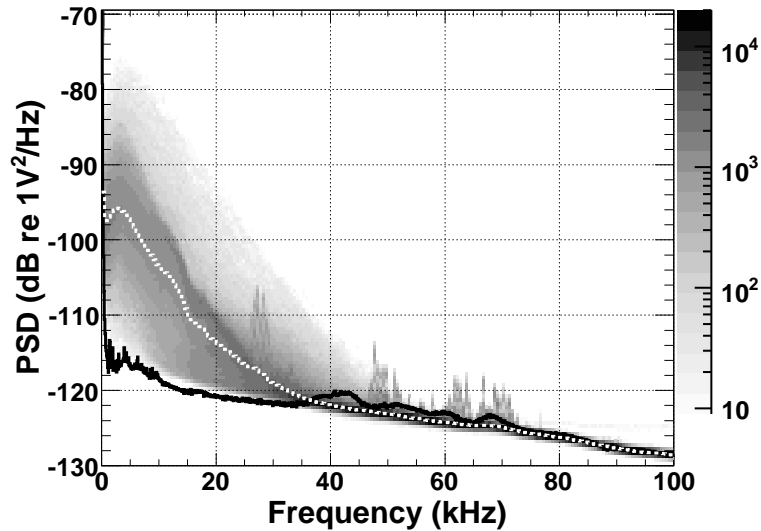


Figure 17. Power spectral density (PSD) of the ambient noise recorded with one HTI sensor on the topmost storey of the IL. The voltage used is the calibrated input voltage of the AcouADC board. Shown in shades of grey is the occurrence rate in arbitrary units, where dark colours indicate higher rates. Shown as a white dotted line is the median value of the in-situ PSD and as a black solid line the noise level recorded in the laboratory prior to deployment.

659 2010 and were received under an angle of about 65° with respect to the direction
 660 pointing vertically upwards. The agreement between the signal shapes can be seen
 661 to be very good. For the second positive peak at about 0.20 to 0.25 s, the AM sensor
 662 shows a differing behaviour from the hydrophones, which can be attributed to the
 663 coupling of the sensor to the glass sphere.

664 Bipolar signals selected with the pulse shape recognition trigger typically have a
 665 signal-to-noise ratio exceeding 2 for a single sensor. Assuming a noise level of
 666 10 mPa in the frequency range from 1 to 50 kHz, which is a typical level recorded
 667 at calm sea, i.e. sea state 0, a signal of 20 mPa can be detected. Such a signal is ex-
 668 pected to be emitted from a 2 EeV cascade emerging from a neutrino interaction at a
 669 distance of about 200 m [3]. Improving the trigger techniques may further enhance
 670 the energy sensitivity. Furthermore, the optimal frequency range must be deter-
 671 mined to maximise the signal-to-noise ratio for pulses stemming from neutrino in-
 672 teractions. To conclude on the feasibility of a large-scale acoustic neutrino detector
 673 in the deep sea—the main objective pursued with the AMADEUS system—further
 674 detailed studies are required.

675 The maximal pressure amplitude that can be recorded for a gain factor of 10 without
 676 saturating the input range of the ADC is about 5 Pa. Usually, only anthropogenic
 677 signals originating close to the detector reach this pressure level at the positions of
 678 the hydrophones.

679 The direction and position reconstruction of acoustic point sources are currently

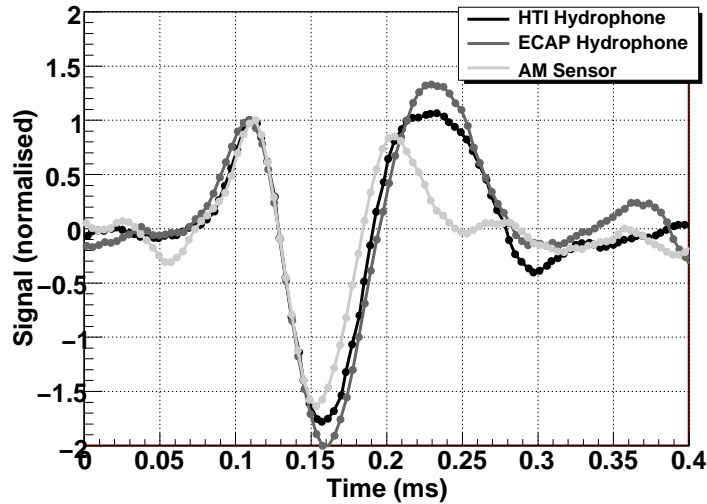


Figure 18. Comparison of the signals originating from a common source as recorded by three different types of acoustic sensors, each one located on a different storey of Line 12. For better comparability, the first peak of each signal has been normalised to 1 and the time axis of each signal adjusted such that the times of the zero crossings between the first positive and negative peak coincide.

680 being pursued as one of the major prerequisites to identify neutrino-like signals.
 681 First results are presented in [15,28].

682 4.4 Position Calibration of Acoustic Storeys

683 Just as for the PMTs in the standard storeys, the relative positions of the acous-
 684 tic sensors within the detector have to be continuously monitored. This is done by
 685 using the emitter signals of the ANTARES acoustic positioning system (see Subsec-
 686 tion 2.1). Figure 19 shows such a signal as recorded by four typical sensors.
 687 The delays between the signal arrival times are clearly visible: short delays of less
 688 than 1 ms within each storey and a long delay of about 10 ms between the signals
 689 arriving in two different storeys.

690 The time shown in the figure is given in seconds since the start of the run and can
 691 be converted into UTC using the data recorded by the clock system (see Subsec-
 692 tion 3.6). As the emission times of the positioning signals are also recorded in UTC,
 693 the time difference between emission and reception of the signal can be calculated.
 694 Using the signals from multiple emitters and their known positions at the anchors
 695 of the lines, the positions of the AMADEUS sensors can be reconstructed.

696 The position calibration has statistical uncertainties of a few millimetres for each
 697 hydrophone. Systematic uncertainties due to the size of the receiving piezo ele-
 698 ments, the knowledge of their relative positions within the acoustic storey, the

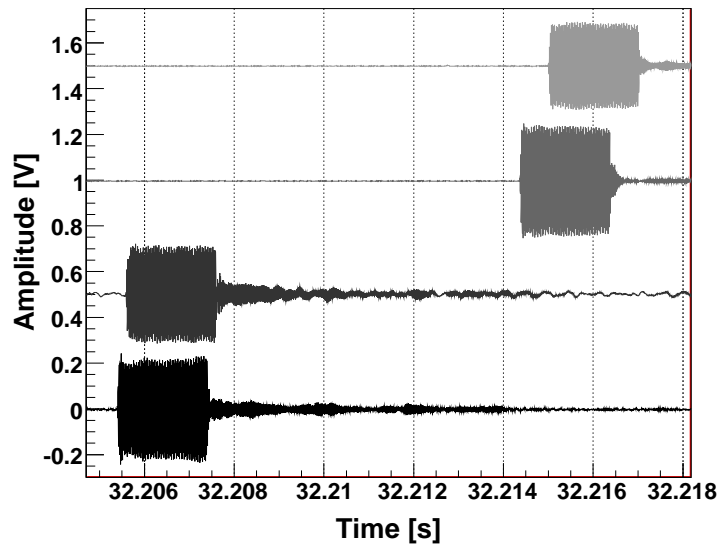


Figure 19. Typical signals of the ANTARES acoustic positioning system as recorded with four sensors of the AMADEUS system for gain factor 1 of the AcouADC board. For better clarity an offset, starting with 0 V and incremented by 0.5 V with respect to the previous one, is added to the amplitude of each sensor. The first two signals along the time axis were recorded by the acoustic storey holding AMs (see Figure 1). The following two signals were recorded with two hydrophones on the acoustic storey just above—one hydrophone mounted at the bottom and the other one at the top of the storey. The time is counted since the start of the run.

699 knowledge of the speed of sound in sea water and the position uncertainties of
 700 the emitters are still under study. For the AMs, the position reconstruction is less
 701 precise and has a statistical uncertainty of the order of a centimetre.

702 5 Summary and Conclusions

703 The AMADEUS system for the investigation of techniques for acoustic particle
 704 detection in the deep sea has been integrated into the ANTARES neutrino telescope
 705 in the Mediterranean Sea at water depths between 2050 and 2300 m. The system
 706 started to take data in December 2007 and was completed in May 2008. It comprises
 707 36 acoustic sensors, of which currently 34 are operational, arranged in six acoustic
 708 clusters. Different configurations of sensor clusters are used. The sensors consist
 709 of piezo-electric elements and two-stage preamplifiers with combined sensitivities
 710 around -145 dB re $1\text{V}/\mu\text{Pa}$.

711 For the off-shore data acquisition, a dedicated electronics board has been designed.
 712 One of 12 steps of analogue amplification between 1 to 562 can be set with the
 713 on-shore control software. Data sampling is done at 500 kSps with 16 bits and

714 an analogue anti-alias filter with a 3 dB point at a frequency of 128 kHz. Digital
715 downsampling with factors of 2 and 4 is implemented inside an off-shore FPGA.
716 This value is also selectable using on-shore control software. The system param-
717 eters were tuned using the data collected with the autonomous precursor device
718 AMADEUS-0 that was deployed and subsequently recovered at the ANTARES
719 site in March 2005.

720 Where appropriate, the components of the AMADEUS system have been calibrated
721 in the laboratory prior to deployment; the in-situ performance is in full accor-
722 dance with the expectations. Data taking is going on continuously and the data
723 are recorded if one of three adjustable trigger conditions is met.

724 The system is well suited to conclude on the feasibility of a future large-scale acous-
725 tic neutrino telescope in the deep sea. Furthermore, it has the potential of a multi-
726 purpose device, combining its design goal to investigate acoustic neutrino detec-
727 tion techniques with the potential to perform marine science studies. AMADEUS
728 is a promising starting point for instrumenting the future neutrino telescope project
729 KM3NeT [29,30] with acoustic sensors for position calibration and science pur-
730 poses.

731 **6 Acknowledgements**

732 The authors acknowledge the financial support of the funding agencies: Centre
733 National de la Recherche Scientifique (CNRS), Commissariat à l'énergie atom-
734 ique et aux énergies alternatives (CEA), Agence National de la Recherche (ANR),
735 Commission Européenne (FEDER fund and Marie Curie Program), Région Alsace
736 (contrat CPER), Région Provence-Alpes-Côte d'Azur, Département du Var and
737 Ville de La Seyne-sur-Mer, France; Bundesministerium für Bildung und Forschung
738 (BMBF), Germany; Istituto Nazionale di Fisica Nucleare (INFN), Italy; Stichting
739 voor Fundamenteel Onderzoek der Materie (FOM), Nederlandse organisatie voor
740 Wetenschappelijk Onderzoek (NWO), the Netherlands; Council of the President of
741 the Russian Federation for young scientists and leading scientific schools support-
742 ing grants, Russia; National Authority for Scientific Research (ANCS), Romania;
743 Ministerio de Ciencia e Innovacion (MICINN), Prometeo of Generalitat Valenciana
744 (GVA) and MULTIDARK, Spain. We also acknowledge the technical support of
745 Ifremer, AIM and Foselev Marine for the sea operation and the CC-IN2P3 for the
746 computing facilities.

747 **References**

748 [1] G.A. Askariyan, B.A. Dolgoshein et al., Nucl. Instr. and Meth. 164 (1979) 267.

- 749 [2] J. Learned, *Phys. Rev. D* 19 (1979) 3293.
- 750 [3] S. Bevan et al. (ACoRNE Coll.), *Astropart. Phys.* 28 (3) (2007) 366, arXiv:astro-
751 ph/0704.1025v1.
- 752 [4] S. Bevan et al. (ACoRNE Coll.), *Nucl. Instr. and Meth. A* 607 (2009) 389,
753 arXiv:0903.0949v2 [astro-ph.IM].
- 754 [5] V. Niess and V. Bertin, *Astropart. Phys.* 26 (2006) 243, arXiv:astro-ph/0511617v3.
- 755 [6] F. Descamps for the IceCube Coll., in: *Proceedings of the 31st International Cosmic*
756 *Ray Conference, 2009*, arXiv:0908.3251v2 [astro-ph.IM].
- 757 [7] K. Antipin et al. (BAIKAL Coll.), in: *Proceedings of the 30th International Cosmic*
758 *Ray Conference, 2007*, arXiv:0710.3113 [astro-ph].
- 759 [8] J. Vandenbroucke, G. Gratta and N. Lehtinen, *Astrophys. J.* 621 (2005) 301,
760 arXiv:astro-ph/0406105.
- 761 [9] S. Danaher for the ACoRNE Coll., in: *Proceedings of ARENA 2006, the 2nd*
762 *International Workshop on Acoustic and Radio EeV Neutrino detection Activities,*
763 *J. Phys. Conf. Ser.* 81, IOP Publishing, Philadelphia, 2007, p. 012011.
- 764 [10] G. Riccobene for the NEMO Coll., in: *Proceedings of ARENA 2008, the 3rd*
765 *International Workshop on Acoustic and Radio EeV Neutrino Detection Activities,*
766 *Nucl. Instr. and Meth. A* 604, 2009, p. 149.
- 767 [11] The ANTARES Collaboration, ANTARES, the first operational Neutrino Telescope in
768 the Mediterranean Sea, to be submitted to *Nucl. Instr. and Meth. A*.
- 769 [12] M. Ageron et al. (ANTARES Coll.), *Astropart. Phys.* 31 (2009) 277, arXiv: 0812.2095
770 v1 [astro-ph].
- 771 [13] P. Amram et al. (ANTARES Coll.), *Nucl. Instr. and Meth. A* 484 (2002) 369.
- 772 [14] M. Ardid for the ANTARES Coll., in: *Proceedings of VLVnT 2008, the 3rd*
773 *International Workshop on a Very Large Volume Neutrino Telescope for the*
774 *Mediterranean Sea, Nucl. Instr. and Meth. A* 602, 2009, p. 174.
- 775 [15] C. Richardt. et al., *Astropart. Phys.* 31 (2009) 19, arXiv:0906.1718v1 [astro-ph.IM].
- 776 [16] M. Ageron et al. (ANTARES Coll.), *Nucl. Instr. and Meth. A* 581 (2007) 695.
- 777 [17] F. Deffner, *Studie zur akustischen Neutrinodetektion: Analyse und Filterung*
778 *akustischer Daten aus der Tiefsee*, Diploma thesis, Univ. Erlangen-Nürnberg, 2007,
779 FAU-PII-DIPL-07-001,
780 obtainable from <http://www.antes.physik.uni-erlangen.de/publications>.
- 781 [18] G. Anton et al., *Astropart. Phys.* 26 (2006) 301.
- 782 [19] K. Graf, *Experimental Studies within ANTARES towards Acoustic Detection of Ultra-*
783 *High Energy Neutrinos in the Deep Sea*, Ph.D. thesis, Univ. Erlangen-Nürnberg, 2008,
784 FAU-PII-DISS-08-001,
785 obtainable from <http://www.antes.physik.uni-erlangen.de/publications>.

- 786 [20] R.J. Urick, Ambient Noise in the Sea, Peninsula publishing, Los Altos, USA, 1986,
787 ISBN 0-932146-13-9.
- 788 [21] C.L. Naumann, Development of Sensors for the Acoustic Detection of Ultra High
789 Energy Neutrinos in the Deep Sea, Ph.D. thesis, Univ. Erlangen-Nürnberg, 2007, FAU-
790 PI4-DISS-07-002,
791 obtainable from <http://www.antares.physik.uni-erlangen.de/publications>.
- 792 [22] J.A. Aguilar et al. (ANTARES Coll.), Nucl. Instr. and Meth. A 570 (2007) 107.
- 793 [23] J.A. Aguilar et al. (ANTARES Coll.), Nucl. Instr. and Meth. A 622 (2010) 59,
794 arXiv:1007.2549v1 [astro-ph.IM].
- 795 [24] R.J. Urick, Principles of Underwater Sound, Peninsula publishing, Los Altos, USA,
796 1983, ISBN 0-932146-62-7.
- 797 [25] J.A. Aguilar et al. (ANTARES Coll.), Astropart. Phys. 26 (2006) 314.
- 798 [26] F. Rademakers and R. Brun, Root: An object-oriented data analysis framework, Linux
799 Journal 51, <http://root.cern.ch/>.
- 800 [27] M. Neff, Studie zur akustischen Teilchendetektion im Rahmen des ANTARES-
801 Experiments: Entwicklung und Integration von Datennahmesoftware, Diploma thesis,
802 Univ. Erlangen-Nürnberg, 2007, FAU-PI1-DIPL-07-003,
803 obtainable from <http://www.antares.physik.uni-erlangen.de/publications>.
- 804 [28] C. Richardt et al., in: Proceedings of ARENA 2008, the 3rd International Workshop
805 on Acoustic and Radio EeV Neutrino Detection Activities, Nucl. Instr. and Meth. A
806 604, 2009, p. 189.
- 807 [29] U.F. Katz et al. (KM3NeT Consortium), in: Proceedings of VLVnT 2008, the
808 3rd International Workshop on a Very Large Volume Neutrino Telescope for the
809 Mediterranean Sea, Nucl. Instr. and Meth. A 602, 2009, p. 40.
- 810 [30] KM3NeT Consortium, Conceptual Design for a Deep-Sea Research Infrastructure
811 Incorporating a Very Large Volume Neutrino Telescope in the Mediterranean Sea,
812 ISBN 978-90-6488-031-5, <http://www.km3net.org/CDR/CDR-KM3NeT.pdf> (2008).